Nuclear Physics **A526** (1991) 415-452
North-Holland

STRANGENESS PRODUCTION IN ANTIPROTON ANNIHILATION AT REST ON ^{3}He, ^{4}He AND ^{20}Ne

F. BALESTRA[1], Yu.A. BATUSOV[2], G. BENDISCIOLI[3,4], S. BOSSOLASCO[5,6], F.O. BREIVIK[7], M.P. BUSSA[5,6], L. BUSSO[5,6], K.M. DANIELSEN[7], C. GUARALDO[8], I.V. FALOMKIN[2], L. FAVA[5,6], L. FERRERO[5,6], V. FILIPPINI[3,4], A. HAATUFT[9], A. HALSTEINSLID[9], T. JACOBSEN[7], E. LODI RIZZINI[6,10], A. MAGGIORA[8], K. MYKLEBOST[9], J.M. OLSEN[9], D. PANZIERI[5,6], G. PIRAGINO[5,6], G.B. PONTECORVO[2], A. ROTONDI[3,4], A.M. ROZHDESTVENSKY[2], P. SALVINI[3,4], M.G. SAPOZHNIKOV[2], S.O. SØRENSEN[7], F. TOSELLO[5,6], V.I. TRETYAK[2], A. VENAGLIONI[3,4] and A. ZENONI[4,11]

[1] *Dipartimento di Scienze Fisiche, Universita di Cagliari, I-09100 Cagliari, Italy*
and
INFN - Sezione di Cagliari, I-09100 Cagliari, Italy
[2] *Joint Institute for Nuclear Research, Dubna, SU-101000 Moscow, USSR*
[3] *Dipartimento di Fisica Nucleare e Teorica, Universita di Pavia, I-27100 Pavia, Italy*
[4] *INFN - Sezione di Pavia, I-27100 Pavia, Italy*
[5] *Istituto di Fisica Generale "A. Avogadro", Universita di Torino, I-10125 Turin, Italy*
[6] *INFN - Sezione di Torino, I-10125 Turin, Italy*
[7] *Physics Department, University of Oslo, N-0316 Oslo 3, Norway*
[8] *Laboratori Nazionali di Frascati dell'INFN, I-00044 Frascati, Italy*
[9] *Physics Department, University of Bergen, N-5007 Bergen, Norway*
[10] *Dipartimento di Automazione Industriale, Universita di Brescia, I-25100 Brescia, Italy*
[11] *CERN/EP, CH-1211 Geneva 23, Switzerland*

Received 15 March 1990
(Revised 20 June 1990)

Abstract: New data are reported on antiproton annihilations at rest with production of Λ and K^0_S, using a streamer chamber with ^{3}He, ^{4}He and ^{20}Ne as gas targets. The data include Λ, K^0_S, ΛK^0_S and $K^0_S K^0_S$ production rates and momentum distributions, π^- momentum spectra, mean numbers of charged particles generally and of negatively charged particles separately for different reaction channels. The yields are compared to simple combinatorial calculations based on the extreme assumptions of Λ production via $B=1$ or via $B=0$ ($\bar{K}$ rescattering) annihilations. Λ and K^0_S momentum spectra are compared to simple model calculations where $B=0$ and $B=1$ annihilations with and without final-state interactions are considered. A review of existing data on Λ and K^0_S production is presented, showing the dependence on the $\bar{p}$ momentum and on the mass number of the target.

E NUCLEAR REACTIONS ^{3,4}He, ^{20}Ne (p-bar, X), E at rest; measured pion momentum spectra, strangeness production, charged particle mean numbers. Gas targets, streamed chamber.

1. Introduction

A process which deposits considerable energy into the nucleus is the absorption of an antiproton. Great interest has been attached to the possible act that, under

appropriate conditions, a collection of nucleons could be transformed into a quark-gluon plasma (QGP). An intensive search for the QGP phase is being done in relativistic heavy-ion collision experiments at Brookhaven and CERN.

The absorption of $\bar{p}$ in nuclei produce initially a more localized "hot spot" and one might ask whether the system subsequently passed through the QGP phase. Rafelski [1]) has argued that the large $\Lambda+\Sigma^0$ production cross section observed in $\bar{p}$ ^{181}Ta reactions at 4 GeV/c [ref. [2])] reflects cold QGP formation. However, it has often been pointed out, for instance by Cugnon *et al.* [3]), that strangeness enhancements are not necessarily signatures of QGP creation, but occur also in a conventional hadronic picture once one includes multinucleon absorption reactions.

Within a more conventional form the strange-particle production below the $\bar{\Lambda}\Lambda$ threshold in nuclei is investigated [4-7]) by means of a cascade-type model where the annihilation is considered to occur on a single nucleon ($B=0$), and where the generation of π, n, ω and kaons is followed by the subsequent rescattering of these particles on the residual nucleons. $B=0$ annihilation produces strangeness in a direct way through $\bar{K}K$ pairs only.

Rescattering allows K^0/K^+ or $\bar{K}^0/K^-$ charge exchange, but allows also the transformation of $\bar{K}^0/K^-$ into hyperons Y ($\bar{K}^0N\rightarrow YX$ or $K^-N\rightarrow YX$), so in addiition to $\bar{K}K$ pairs rescattering allows production of KY pairs. Moreover, rescattering of other particles increases somewhat the total strange-particle yield, mainly due to ωN rescattering [6]).

Annihilation on more than one nucleon ($B>0$ annihilation) can also produce $K\bar{K}$ and KY pairs, and the total strange-particle yield is higher in this channel than in the $B=0$ case before rescattering [3]). For $B=1$ annihilations at rest, ref. [8]) predicts that the strange particles are produced at a rate of 17.1% compared to 4.7% for the $B=0$ annihilations. Moreover, in the annihilations on ^{3}He and ^{4}He above 400 MeV/c the $B=1$ annihilations should give a rate of about 10% [ref. [8])]. A probability of the same magnitude seems to come out of experiments with annihilations at rest on deuterium [9,10]).

Of course, rescattering can occur also after $B=1$ annihilations, with similar effects as those described for $B=0$ case. In any case, the presence of hyperons among the final products of anti-proton nucleus annihilations in this energy region reveals that processes exist which involve more than one nucleon. Kaons, on the other hand, can also be generated in processes on single nucleons.

This paper is intended to contribute to the understanding of the production of K^0_S and $\Lambda(\Sigma^0)$ in annihilations of antiproton at rest on ^{3}He, ^{4}He and ^{20}Ne nuclei. In particular we shall consider ratios like

$$R=\frac{N(\Lambda)+N(\Sigma^0)}{N(K^0_S)}, \qquad R_\Lambda=\frac{N(\Lambda)+N(\Sigma^0)}{N(\text{inelastic events})}, \qquad R_{K^0_S}=\frac{N(K^0_S)}{N(\text{inelastic events})},$$

which should indicate the relative importance of the multinucleon processes. For pure $B=1$ annihilations at rest the ratio R has been estimated to be 1.46 [ref. [8])].

For $B=0$ annihilation plus rescattering the ratio R has been estimated to be 1.10 for ^{12}C below 400 MeV/c and 1.43 for ^{20}Ne at 600 MeV/c [ref. [6])].

There have been essentially six experiments investigating strange particle production in $\bar{p}$ reactions on nuclei heavier than deuterium: Miyano *et al.* at 4 GeV on ^{181}Ta in a bubble chamber at KEK [refs. [2,11])], the PS 179 collaboration at 0.6 GeV/c on ^{20}Ne and ^{4}He in a streamer chamber at LEAR, CERN [refs. [12,13])], Condo *et al.* at 0.0–0.4 GeV/c on C, T, Ta and Pb [ref. [14])], Smith *et al.* at rest on C and U [ref. [15])] Barmin *et al.* at 0.3–1.05 GeV/c and at rest on ^{131}Xe [ref. [16])] and ASTERIX at rest on ^{14}N [ref. [17])].

In ref. [12]) we presented results on neutral strange-particle production in annihilations of $\bar{p}$ on ^{20}Ne at 607 MeV/c. In this work we extend the analysis to include

$$\bar{p}+{}^{20}Ne \to V^0+X \qquad \text{at rest}$$

$$\bar{p}+{}^{4}He \to V^0+X \qquad \text{at rest}$$

$$\bar{p}+{}^{3}He \to V^0+X \qquad \text{at rest}$$

where $V^0=\Lambda(\Sigma^0)$ or K^0_S.

The experimental apparatus consisted of a self-shunted streamer chamber in a magnetic field and was exposed to the $\bar{p}$ beams of LEAR facility at CERN. The details of the apparatus and its performance are reported in ref. [18]). The chamber has a sensitive volume of $70\times90\times18$ cm^3. The magnetic field was 0.5 T (^{20}Ne) and 0.4 T (^{4}He and ^{3}He). The beam was degraded from 105 MeV/c down to $\approx$61 MeV/c to make the $\bar{p}$ stop in the central region of the gas target.

The paper is organized as follows: sect. 2 is devoted to the Λ and K^0_S yields. In sect. 2.1 we evaluate the values of R_Λ, $R_{K^0_S}$ and R for ^{3}He, ^{4}He and ^{20}Ne at rest and in sect. 2.2 the yields of $K^0_S\Lambda$ and $K^0_SK^0_S$ events. In sect. 2.3 we compare our data with the whole world set of similar data at rest and in flight. Beside Λ and K^0_S yields, this review considers mean values of momenta, rapidities and prong multiplicities. In sect. 2.4 we make an analysis of data based on simple assumptions in order to see whether the data are consistent with Λ being produced in pure $B=0$ or $B=1$ annihilations.

Sect. 3 is devoted to the momentum spectra of Λ, K^0_S and π^- and to charged particles multiplicities. In sect. 3.1 we show the momentum distributions of Λ, K^0_S and π^- (produced mainly in annihilation events without strangeness) on ^{3}He, ^{4}He and ^{20}Ne at rest. In sect. 3.2 we introduce simple models to analyse the data.

2. Λ and K^0_S yields

2.1. MEASUREMENTS OF R_Λ, $R_{K^0_S}$ AND R

Λ and K^0_S were observed through their charged decay modes:

$$\Lambda \to p\pi^- \quad (64.1\%), \qquad K^0_S \to \pi^+\pi^- \quad (68.6\%).$$

Each annihilation with at least one associated V^0 candidate was fully measured and processed through the Hydra geometry and kinematic program. No distinction could be made between Λ and Σ^0. In order to select between Λ and K^0_S we use the following selection criteria:

(a) In the case of ambiguity between Λ and K^0_S we select the hypothesis with the highest probability of the kinematic fit. This method was used in $\bar{p}$ ^{4}He and $\bar{p}$ ^{20}Ne only.

(b) For $\bar{p}$ ^{3}He we do the selection, whenever possible, according to ionisation or production of a deuteron. Distinction between deuterons, protons and π^+ is possible in ^{3}He (and ^{4}He, ref. [18])) for tracks with momenta <450 MeV/c and dip angle $<40°$. Note that if a deuteron d is produced in $\bar{p}$ ^{3}He $\rightarrow$ d X, then X cannot contain a Λ due to conservation of baryon number. Similarly in $\bar{p}$ ^{4}He $\rightarrow$ ^{3}He X which are even prong events, and $\bar{p}$ ^{4}He $\rightarrow$ ^{3}H X (odd prong events), X cannot contain a Λ.

The selection criterion (a) introduced a background of $\Lambda(K^0_S)$ in the $K^0_S(\Lambda)$ sample. In order to estimate this background a Monte Carlo program was made where genuine Λ and K^0_S are distorted according to the errors coming from the Hydra geometry program. The $\Lambda(K^0_S)$ sample was taken from the fitted $\Lambda(K^0_S)$ events. The distorted Λ and K^0_S are subsequently processed through the Hydra kinematic program in the same way as the experimental events. The probability of selecting the wrong hypothesis through criterion (a) turns out to be $\approx$10%. However, the corrections necessary in R, R_Λ and $R_{K^0_S}$ turn out to be about 2% or less, since the number of events transferred from Λ to K^0_S is about the same as that transferred from K^0_S to Λ.

From fig. 1a and fig. 1b we see that there is a substantial loss in V^0 events with short decay lengths here shown. This is due to bad visibility near the primary vertex. Using the experimental momentum spectra (without cuts in decay length) together with the number of events with decay length $L>1$ cm we can estimate correction factors $X = N_{tot}/N_{L>1}$ to be (1.76 ± 0.25) (Λ) and (1.60 ± 0.20) (K^0_S) for ^{20}Ne, (1.76 ± 0.15) (Λ) and (1.63 ± 0.13) (K^0_S) for ^{4}He and $(1.85\pm0.15$ (Λ) and (1.63 ± 0.13) (K^0_S) for ^{3}He. (The dashed lines in fig. 1a and fig. 1b have been calculated using the corrected total number of events N_{tot} and the experimental momentum spectra of Λ and K^0_S). This method might lead to a systematic underestimation of the total number of events due to a possible lack of low momentum events in the experimental momentum spectra. However, in order to investigate this further, we try to estimate X by using models (see sect. 3).

In fig. 19b and fig. 17a we have compared the experimental momentum distributions of Λ and K^0_S with model predictions. In the experimental data we have made a cut at 1 cm in the decay length, and the model predictions are weighted accordingly. The model reproduces the momentum distributions fairly well, and we estimate X to be 1.85 ± 0.04 (Λ) and 1.71 ± 0.04 (K^0_S), consistent with values of X given above.

In table 1 we present the total number of antiprotons $N_{\bar{p}}$, the number of events detected, the number of events with $L>1$ cm and the corrected numbers N_{tot}. Finally

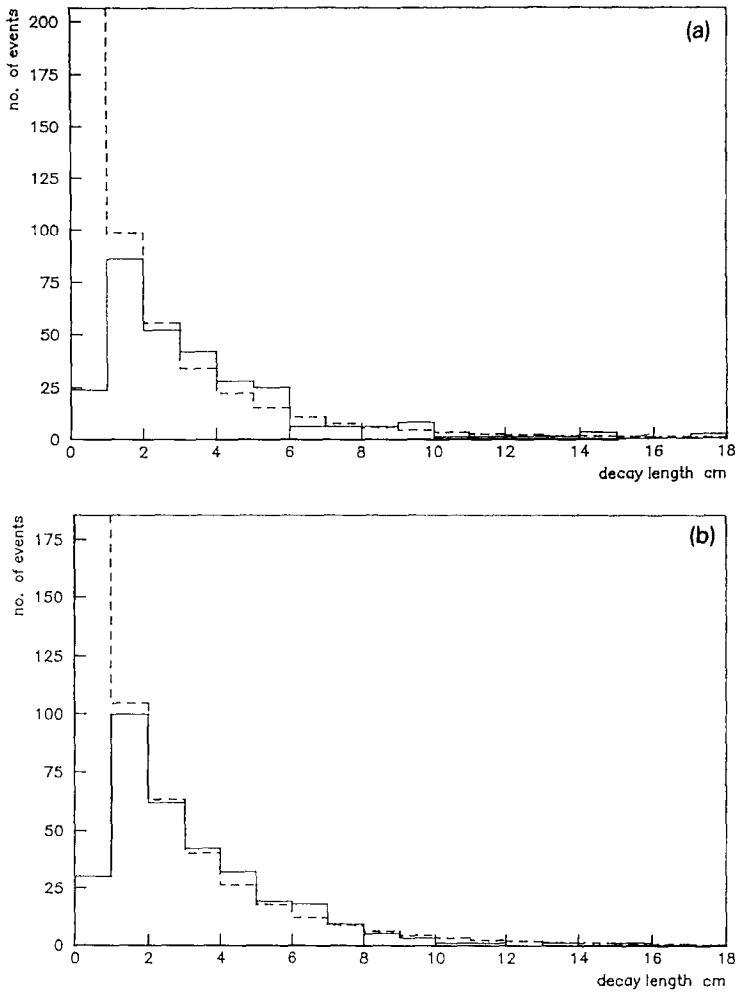

Fig. 1. (a) Distribution of decay lengths for Λ in ^{4}He. (b) Distribution of decay lengths for K^0_S in ^{4}He. Solid line: experiment; dashed line: calculated.

TABLE 1

Total number of antiprotons $N_{\bar{p}}$ and number of produced Λ and K^0_S in $\bar{p}$ ^{3}He, $\bar{p}$ ^{4}He and $\bar{p}$ ^{20}Ne at rest: (a) No decay length (L) cut, (b) $L > 1$ cm, (c) numbers of Λ and K^0_S corrected for loss in chamber

	$\bar{p}$ ^{3}He at rest				p ^{4}He at rest				$\bar{p}$ ^{20}Ne at rest			
	$N_{\bar{p}}$	No L cut	$L>1$ (cm)	Corr.	$N_{\bar{p}}$	No L cut	$L>1$ (cm)	Corr.	$N_{\bar{p}}$	No L cut	$L>1$ (cm)	Corr.
$N(\Lambda)$	14319	28	27	50±9	72645	292	268	472±49	30364	103	87	153±27
$N(K^0_S)$		101	96	156±16		325	295	481±47		93	85	136±25

corrections for neutral decay modes of Λ and K^0_S, unmeasurable events (9%), wrong solutions ($\leq$2%) and scanning efficiency (98%) are taken into account to give the results presented in table 2.

2.2. $K^0_S K^0_S$ AND ΛK^0_S YIELDS

In $\bar{p}$ ^{4}He annihilations at rest, where the statistics are highest, we found 42 events with 2 visible V^0: $27\Lambda K^0_S$, $9K^0_S K^0_S$ and $6\Lambda\Lambda$. First we notice that the number of $\Lambda\Lambda$ events is consistent with the $\approx$10% wrong solutions coming from the kinematic fit selection. Therefore we consider the $\Lambda\Lambda$ events to be ΛK^0_S. After correction for wrong solutions we have $11K^0_S K^0_S$ and $31\Lambda K^0_S$.

2.3. AN EXPERIMENTAL REVIEW

A review of existing data on R, R_Λ and $R_{K^0_S}$ where K^0_S and Λ are produced in $\bar{p}$-nucleus annihilations are given in table 3 together with the corresponding values from $\bar{p}p$ and $\bar{p}d$ annihilations. Although the data on strange-particle production in $\bar{p}$ nucleus annihilations are rather limited we can make the following observations from table 3:

2.3.1. Annihilations at rest.

(a) Λ production:

(i) R_Λ is about 1% when $A \geq 4$.

(ii) $R_\Lambda(A \geq 4) > R_\Lambda(^3\mathrm{He}) > R_\Lambda(^2\mathrm{H})$.

(iii) $R_\Lambda(A \geq 4)$ is about 3 times $R_\Lambda(^2\mathrm{H})$.

The errors are too large to determine how R_Λ depends on A for $A > 4$.

(b) K^0_S production:

$$R_{K^0_S}(^1\mathrm{H}) \sim R_{K^0_S}(^2\mathrm{H}) > R_{K^0_S}(^3\mathrm{He}) > R_{K^0_S}(^4\mathrm{He}) > R_{K^0_S}(^{20}\mathrm{Ne})\,.$$

The lower values of R_Λ and R for ^{2}H and ^{3}He may reflect that these nuclei have a loose structure in disfavour of rescattering and/or multinucleon annihilation. In

TABLE 2

Yield of Λ and K^0_S (per $\bar{p}$), R_Λ(%), $R_{K^0_S}$(%) and Λ/K^0_S ratio (R) in $\bar{p}$ ^{3}He, $\bar{p}$ ^{4}He and $\bar{p}$ ^{20}Ne at rest

	$\bar{p}$ ^{3}He at rest	$\bar{p}$ ^{4}He at rest	$\bar{p}$ ^{20}Ne at rest
R	0.35 ± 0.08	1.05 ± 0.16	1.18 ± 0.29
R_Λ (%)	0.55 ± 0.11	1.12 ± 0.12	0.85 ± 0.15
$R_{K^0_S}$ (%)	1.59 ± 0.20	1.07 ± 0.11	0.72 ± 0.12

TABLE 3

Review of experimental data on the yield of Λ (R_Λ) and K^0_S ($R_{K^0_S}$) (per $\bar{p}$) for different targets and different antiproton momenta (Note that $R_{K^0_S}$ for deuterium at rest is the average of hydrogen and neutron. The latter has been calculated from data in ref. [37]))

	0	450	600	1600	3000	4000	4600	9100
R_Λ (%)								
^1H	0.36 ± 0.06 [9])	-	-	0.15 ± 0.02 [10,30,31])	0.66 ± 0.11 [10,30,31])	1.05 ± 0.10 [10,19])	1.52 ± 0.14 [19,21])	2.6 ± 0.27 [19,21])
^2H	0.30 ± 0.04 [17])	0.33 ± 0.08 [33,34,35])	0.42 ± 0.09 [33,34,35])	0.55 ± 0.05 [10,31])	0.72 ± 0.07 [10,31])			
^3He	0.55 ± 0.11 [a])							
^4He	1.12 ± 0.15 [13])		1.53 ± 0.22 [13,20])					
^{12}C	2.3 ± 0.6 [14])							
^{14}N	0.62 ± 0.02 [17])							
^{20}Ne	0.85 ± 0.15 [a])		1.95 ± 0.43 [12])					
^{48}Ti	2.1 ± 0.7 [14])							
^{131}Xe	2.46 ± 0.30 [16]) [b])		3.13 ± 0.30 [16]) [b,c])					
^{181}Ta	1.3 ± 0.4 [14])				8.76 ± 0.61 [36])	11.85 ± 0.74 [11])		
^{208}Pb	2.7 ± 1.1 [14])							
$R_{K^0_S}$ (%)								
^{1}H	2.03 ± 0.08 [37])			3.71 ± 0.14 [10,30,31])	3.77 ± 0.05 [10,30,31])	3.77 ± 0.16 [11,31])	4.66 ± 0.34 [31,32])	5.0 ± 0.34 [31,32])
^{2}H	1.97 ± 0.10	1.55 ± 0.31 [33,34,35])	2.42 ± 0.36 [33,34,35])	2.86 ± 0.16 [10,31])	2.46 ± 0.15 [10,31])			
^{3}He	1.59 ± 0.20 [a])							
^{4}He	1.07 ± 0.11 [a])		1.63 ± 0.22 [20])					
^{20}Ne	0.72 ± 0.12 [a])		0.85 ± 0.17 [12])					
^{131}Xe	2.14 ± 0.23 [16]) [b])		1.99 ± 0.18 [16]) [b,c])					
^{181}Ta					2.62 ± 1.21 [36])	5.03 ± 0.37 [11])		
R								
^{1}H				0.07 ± 0.01	0.17 ± 0.03	0.28 ± 0.03	0.32 ± 0.04	
^{2}H	0.16 ± 0.02	0.21 ± 0.07	0.17 ± 0.05	0.19 ± 0.04	0.29 ± 0.03			
^{3}He	0.35 ± 0.08							
^{4}He	1.05 ± 0.14		0.94 ± 0.19					
^{20}Ne	1.18 ± 0.29		2.3 ± 0.7					
^{131}Xe	1.15 ± 0.19		1.57 ± 0.20					
^{181}Ta					3.34 ± 1.56	2.35 ± 0.22		

[a]) This work.
[b]) Preliminary results.
[c]) Average 400 to 900 MeV/c.

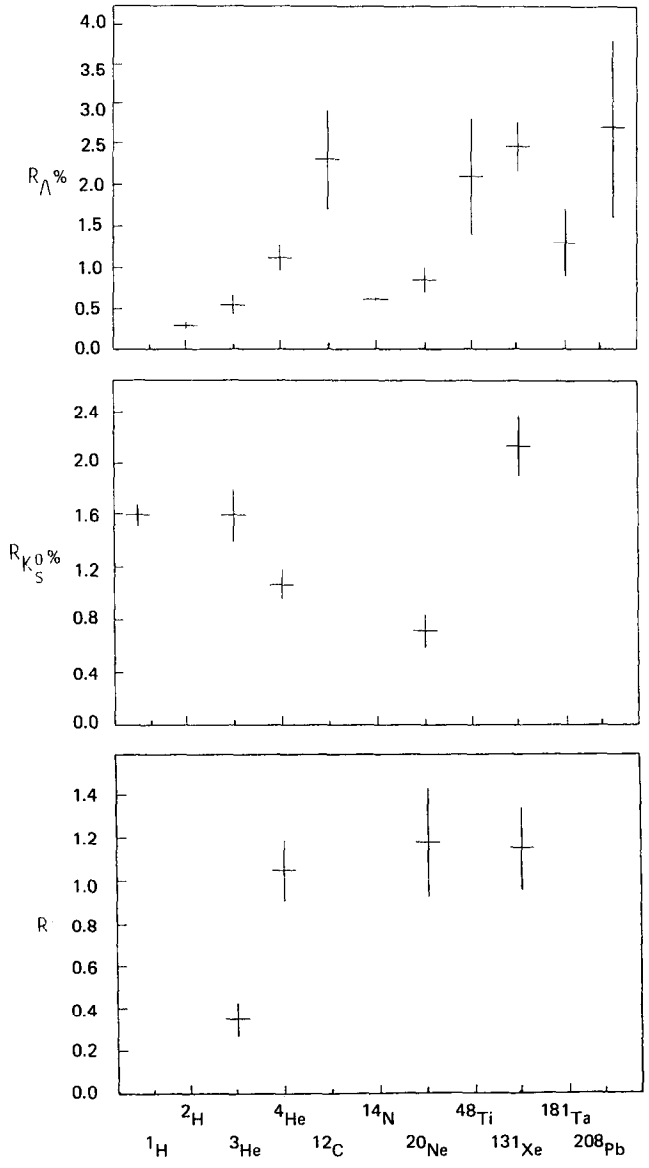

Fig. 2. Distribution of R_Λ, $R_{K^0_S}$ and R for different experiments on $\bar{p}A \to V^0$ X at rest ($V^0 = K^0_S$ or Λ).

fig. 2 we show the distribution of R_Λ, $R_{K^0_S}$ and R for different experiments on $\bar{p}A \to V^0$ X at rest (V^0 is K^0_S or Λ).

2.3.2. Annihilations in flight below 1600 MeV/c.

(a) $R_\Lambda(^2H)$ and $R_{K^0_S}(^2H)$ increase with momentum in such a way that R stays almost constant.

(b) R_Λ increases as a function of A.

(c) R_Λ at 600 MeV/c is larger than the corresponding value at rest.

(d) $R(^2\mathrm{H})$ stays constant with increasing momentum and is about one order of magnitude smaller than $R(A \geq 4)$.

2.3.3. Annihilation above 1600 MeV/c.

(a) Above $\bar{\Lambda}\Lambda$ threshold $R_\Lambda(^1\mathrm{H})$ increase with energy while $R_{\mathrm{K}^0_S}(^1\mathrm{H})$ is fairly constant. At 9 GeV/c, $R_\Lambda(^1\mathrm{H}) \approx \frac{1}{2} R_{\mathrm{K}^0_S}(^1\mathrm{H})$. A similar behaviour is observed for $R_\Lambda(^2\mathrm{H})$ and $R_{\mathrm{K}^0_S}(^2\mathrm{H})$.

(b) $R_\Lambda(^2\mathrm{H})$ and $R_{\mathrm{K}^0_S}(^2\mathrm{H})$ vary smoothly through the $\bar{\Lambda}\Lambda$ threshold, contrary to the situation for $R_\Lambda(^{181}\mathrm{Ta})$ which is about one order of magnitude larger at 3–4 GeV/c than at rest.

(c) $R_\Lambda(^{181}\mathrm{Ta})$ at 3–4 GeV/c is one order of magnitude larger than $R_\Lambda(^1\mathrm{H})$ and $R_\Lambda(^2\mathrm{H})$ at the same momenta. On the other hand, $R_{\mathrm{K}^0_S}$ depends moderately of A. Some processes in ^{181}Ta increase strongly the Λ production without reducing the K^0_S yield.

(d) $R_{\mathrm{K}^0_S}(^2\mathrm{H}) < R_{\mathrm{K}^0_S}(^1\mathrm{H})$, and this is not sufficiently balanced by $R_\Lambda(^2\mathrm{H}) > R_\Lambda(^1\mathrm{H})$. In table 4 we present the current experimental situation concerning the total inelastic cross section $\sigma_{\mathrm{in}} = \sigma_{\mathrm{tot}} - \sigma_{\mathrm{el}}$. We infer that σ_{in} behaves as $A^{2/3}\ \sigma_{\mathrm{in}}(^1\mathrm{H})$ (number in parenthesis) over a large range of A and of $\bar{\mathrm{p}}$ momentum. From table 5 we see that σ_Λ and $\sigma_{\mathrm{K}^0_S}$ deviate strongly from such a behaviour [2]).

In table 6 we present a review of kinematical quantities, charge multiplicities and multiplicities of negative tracks (π^- and K^-) where we can make the following observations:

– The average number of charged particles N_{ch} and of negative particles N_{π^-} are higher for annihilation events in general (all types) than for those with Λ or/and K^0_S. This reflects the fact that events with strange particle production have less energy available for production of $\pi^\pm$.

TABLE 4

Total inelastic cross sections in $\bar{\mathrm{p}}$ A reactions. The value for ^{20}Ne is underestimated by ≈5% [ref. [39])]. Numbers in parentheses from $\sigma_{\mathrm{in}} = A^{2/3}\ \sigma_{\mathrm{in}}(^1\mathrm{H})$

	σ(mb)		
	600 MeV/c	3000 MeV/c	4000 MeV/c
^{1}H	94.7 ± 2.4 [38])	53 ± 1 [31])	50.4 ± 1.2 [31])
^{2}H	162.8 ± 3.1 [34])	≈113 [31])	
^{4}He	239 ± 5 [20])		
	(238 ± 6)		
^{20}Ne	623 ± 21 [39])		
	(698 ± 18)		
^{181}Ta		1656 ± 30 [36])	1628 ± 30 [11])
		(1696 ± 32)	(1613 ± 38)

TABLE 5

Cross sections of Λ and K^0_S in $\bar{p}$ A annihilations

	600 MeV/c			4 GeV/c	
	^{2}H [ref. [33])]	^{4}He [ref. [12])]	^{20}Ne [ref. [12])]	^{1}H [ref. [11])]	^{181}Ta [ref. [11])]
σ_Λ(mb)	0.65 ± 0.14	3.67 ± 0.56	12.3 ± 2.8	0.53 ± 0.05	193 ± 12
$\sigma_{K^0_S}$(mb)	3.74 ± 0.56	3.90 ± 0.53	5.4 ± 1.1	1.90 ± 0.07	82 ± 6

– N_{ch} for events with Λ is higher than for those with K^0_S which may reflect that the nucleus is more strongly involved.
– Note that we can only state the lower limits of N_{ch} for $\bar{p}$ ^{181}Ta at 4 GeV/c. The reason is that prongs with momentum less than 100 MeV/c cannot be observed in that experiment. Since in our experiment we are using a gas target we are able to detect such prongs and we have indeed quite a lot of them [19,20]).

2.4. DATA ANALYSIS

We shall first assume that all Λ are produced through $\bar{K}$ rescattering, in the processes

$$\bar{p}N \to \bar{K}K(m\pi) \qquad m = 0, 1, 2 \ldots$$

followed by

$$\bar{K}N \to \Lambda X ,$$

with a certain probability $P_{\bar{K}\to\Lambda}$ of $\bar{K}$ converting to Λ in the nucleus. Assuming a $P_{\bar{K}K}$ rate as given above we can calculate $P_{\bar{K}\to\Lambda}$ as

$$P_{\bar{K}\to\Lambda} = (R_\Lambda)_{exp} / P_{\bar{K}K} .$$

$P_{\bar{K}\to\Lambda}$ is an estimate of the average value of the probabilities $P_{\bar{K}^0\to\Lambda}$ and $P_{K^-\to\Lambda}$ that $\bar{K}^0$ or K^- convert to a Λ in the nucleus. If $P_{\bar{K}\to\Lambda}$ is known we can estimate R based on the following assumptions:
– The production of $\bar{K}K$, together with any number of pions, has a probability $P_{\bar{K}K}$ of about 5–7% with respect to the total number of events in $\bar{N}N$ annihilations at rest [5]). In ref. [21]) a value of $P_{\bar{K}K} = 3\%$ is found in antiproton-nucleus annihilations. We therefore assume the $P_{\bar{K}K}$ rate to be 3% (or alternatively 5%) at rest.

We calculate $R = (R_\Lambda)_{exp} / R_{K^0_S}$ for both these two alternatives. As in ref. [22]) we assume $P_{\bar{K}K}$ to increase linearly as a function of the antiproton momentum, i.e. at 607 MeV/c we put $P_{\bar{K}K} = 4.5\ (6.5)\%$.

TABLE 6

Review of kinematical quantities, mean charge multiplicities $\langle N_{ch} \rangle$ and multiplicities $\langle N_- \rangle$ of negative tracks (π^- and K^-). The mean momenta of Λ and K^0_S in $\bar{p}$ ^{20}Ne and p ^{4}He are given with (numbers in parentheses) and without L cut. (Note that one can only state a lower limit for N_{ch} in $\bar{p}$ ^{181}Ta at 4 GeV/c, since prongs with momenta less than 100 MeV/c cannot be observed in that experiment)

		Ref.	y	$\langle p \rangle$ MeV/c	$\langle p_\perp \rangle$ MeV/c	$\langle p_L \rangle$ MeV/c	$\langle N_{ch} \rangle$	$\langle N_{\pi^-} \rangle$
^{20}Ne	Λ	[12]	0.07 ± 0.03	365 ± 22	263 ± 17	116 ± 29	6.1 ± 0.3	
607 MeV/c	π^-_Λ	[12]	0.31 ± 0.08	297 ± 27	259 ± 29	111 ± 32		1.05 ± 0.10
	K^0_S	[12]	0.33 ± 0.07	508 ± 24	331 ± 25	239 ± 41	5.5 ± 0.3	
	$\pi^-_{K^0_S}$	[12]	−0.01 ± 0.06	270 ± 26	304 ± 35	3 ± 24		1.19 ± 0.10
	π^-	[19]	0.25 ± 0.02	334 ± 4	289 ± 5	106 ± 6	6.60 ± 0.05	1.37 ± 0.04
^{4}He	Λ	[13]	0.07 ± 0.03	433 ± 33	354 ± 30	86 ± 38		
607 MeV/c	π^-_Λ	[13]	0.37 ± 0.13	366 ± 37	253 ± 31	148 ± 44		1.09 ± 0.10
	K^0_S	[13]	0.35 ± 0.06	555 ± 35	393 ± 30	254 ± 44		
	$\pi^-_{K^0_S}$	[13]	0.43 ± 0.11	395 ± 34	264 ± 24	165 ± 43		1.27 ± 0.09
	π^-	[20]					4.18 ± 0.07	1.66 ± 0.03
^{20}Ne				(344 ± 20)				
at rest	Λ			317 ± 19			4.71 ± 0.20	
	π^-_Λ			235 ± 19				1.05 ± 0.09
				(478 ± 21)				
	K^0_S			468 ± 21			4.02 ± 0.22	
	$\pi^-_{K^0_S}$			255 ± 22				1.01 ± 0.10
	π^-	[19]		320 ± 7			5.60 ± 0.04	1.50 ± 0.03
^{4}He				(333 ± 12)				
at rest	Λ			320 ± 11			3.03 ± 0.08	
	π^-_Λ			294 ± 12				1.03 ± 0.05
				(445 ± 11)				
	K^0_S			437 ± 10			2.72 ± 0.07	
	$\pi^-_{K^0_S}$			297 ± 12				0.97 ± 0.05
	π^-	[39]		334 ± 3			4.10 ± 0.13	1.65 ± 0.03
^{3}He				(347 ± 39)				
at rest	Λ			340 ± 38			2.76 ± 0.27	
	π^-_Λ							0.88 ± 0.13
				(403 ± 19)				
	K^0_S			398 ± 19			2.97 ± 0.14	
	$\pi^-_{K^0_S}$							0.99 ± 0.07
	π^-	[20]		333			4.17 ± 0.08	1.58 ± 0.03
^{181}Ta	Λ	[2]						
4 GeV/c			0.24		370		> 5.66 ± 0.03	
	π^-_Λ	[2]						1.13 ± 0.03
	K^0_S	[2]	0.6		340		> 5.14 ± 0.03	
	$\pi^-_{K^0_S}$	[2]						1.25 ± 0.03
	π^-						5.66 ± 0.03	1.44 ± 0.04

– The branching ratios of different charge configurations for $\bar{K}K$-pairs are taken from ref. [21]) ($K^+\bar{K}^0$ (16%), K^+K^- (27%), $\bar{K}^0K^0$ (27%) and K^0K^- (30%)).

– We neglect charge-exchange of (anti)kaons.

– The $\bar{K}$ is the only particle which produces Λ through rescattering (neglecting contributions from, for instance, ωN rescattering).

Hence by these assumptions we get

$$P_{K^0_S} = P_{\bar{K}K}\{\tfrac{1}{2}(K^0K^-) + \tfrac{1}{2}P_{\bar{K}\to\Lambda}(\bar{K}^0K^0) + (1 - P_{\bar{K}\to\Lambda})[\bar{K}^0K^0 + \tfrac{1}{2}(K^+\bar{K}^0)]\}\,.$$

TABLE 7

Prediction of the absorption rate $P_{\bar{K}\to\Lambda}$ and $\Lambda/K^0_S(R)$ ratio assuming production of Λ from $B=0$ fireball only. Numbers in parentheses are based on $P_{\bar{K}K}=0.05$ instead of 0.03 at rest

	$\bar{p}$ ^{3}He at rest	$\bar{p}$ ^{4}He at rest	$\bar{p}$ ^{20}Ne at rest	$\bar{p}$ ^{4}He 607 MeV/c	$\bar{p}$ ^{20}Ne 607 MeV/c
$P_{\bar{K}\to\Lambda}$	0.18 ± 0.04	0.37 ± 0.04	0.28 ± 0.05	0.34 ± 0.05	0.43 ± 0.09
	(0.11 ± 0.02)	(0.22 ± 0.02)	(0.17 ± 0.03)	(0.24 ± 0.04)	(0.30 ± 0.06)
R	0.40	0.89	0.64	0.80	1.06
	(0.23)	(0.50)	(0.37)	(0.52)	(0.67)
R_{exp}	0.35 ± 0.08	1.05 ± 0.14	1.18 ± 0.25	0.94 ± 0.19	2.3 ± 0.7

Then R is given by

$$R=(R_\Lambda)_{exp}/R_{K^0_S}.$$

The results are presented in table 7.

Since $R=11.85$ in $\bar{p}$ ^{181}Ta at 4 GeV/c [ref. [2])], then $P_{\bar{K}K}>12\%$ in order that $P_{\bar{K}\to\Lambda}<1$. Assuming $P_{\bar{K}K}=3(5)\%$ at rest and an energy dependence as given in ref. [22]) we get $P_{\bar{K}K}=13\,(15)\%$ at 4 GeV/c. Using these values we get $P_{\bar{K}\to\Lambda}=0.91\,(0.79)$ and values of $R=3.0\,(2.4)$.

We could take the opposite approach and assume that fireballs of baryon number $B=1$ are formed in antiproton-nucleus annihilation. Then we must expect a noticeable fraction of Λ and Σ produced by the $B=1$ fireballs [3,8]). In this model, however, the formation probability P_f of such fireballs is very uncertain. In order to establish an upper limit for the probability P_f we assume:

– The fraction of Λ produced in $B=1$ annihilations, P_Λ, is taken to be 7.6% [ref. [8])] where we have included Σ^0.

– We neglect the $\Sigma^\pm\to\Lambda$ conversion in the nucleus.

– We neglect any influence of the nucleus on the produced Λ.

Hence $P_f<(R_\Lambda)_{exp}/P_\Lambda$. The results are shown in table 8.

In table 8 we also show an estimation of R based on the following assumptions:

– For P_f we use the upper limit (i.e. we put the probability of Λ production through rescattering of $\bar{K}$ equal to zero).

TABLE 8

Upper limit of $B=1$ fireball production P_f and predicted $\Lambda/K^0_S(R)$ ratio assuming production from $B=1$ fireball only. Numbers in parentheses are based on $P_{\bar{K}K}=0.05$ instead of 0.03 at rest

	$\bar{p}$ ^{2}H at rest	$\bar{p}$ ^{3}He at rest	$\bar{p}$ ^{4}He at rest	$\bar{p}$ ^{20}Ne at rest	$\bar{p}$ ^{2}H 600 MeV/c	$\bar{p}$ ^{4}He 607 MeV/c	$\bar{p}$ ^{20}Ne 607 MeV/c
$P_f(\%)$	$\leq4.7\pm0.8$	$\leq7.2\pm1.4$	$\leq14.7\pm1.2$	$\leq11.2\pm2.3$	≤5.5	$\leq20.1\pm2.5$	$\leq25.6\pm6.4$
R	0.22 (0.14)	0.32 (0.22)	0.59 (0.41)	0.47 (0.32)	0.18 (0.13)	0.58 (0.44)	0.71 (0.56)
R_{exp}	≈0.2	0.35 ± 0.08	1.05 ± 0.14	1.18 ± 0.25	0.17 ± 0.05	0.94 ± 0.19	2.3 ± 0.7

– The branching ratios of different charge configurations for $\bar{K}K$ pairs are as given above.

– The probability to produce a K_S^0 from a $B=1$ fireball is taken from ref. [3]) (4.2%).

Hence we have

$$R_{K_S^0} = P_f P_{K_S^0}(B=1) + P(B=0) P_{K_S^0}(B=0)\,,$$

where

$$P(B=0) = 1 - P_f\,,$$

$$P_{K_S^0}(B=0) = P_{\bar{K}K}(B=0)\{\tfrac{1}{2}(K^+\bar{K}^0) + \tfrac{1}{2}(K^0K^-) + (\bar{K}^0K^0)\}\,.$$

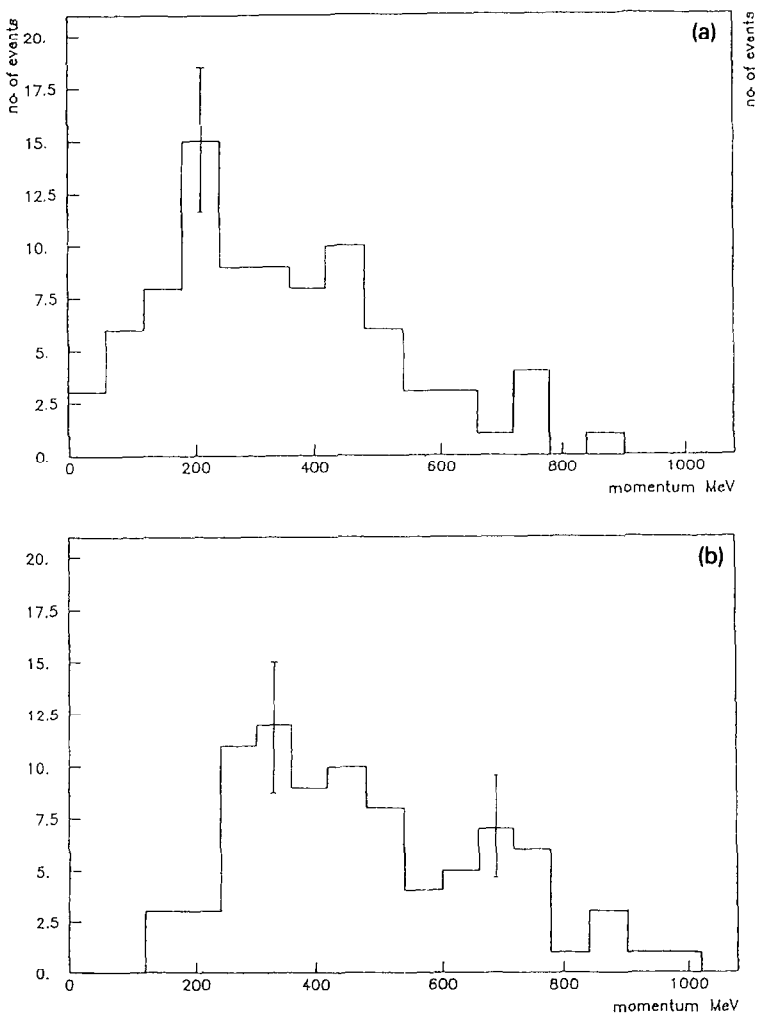

Fig. 3. (a) Momentum spectrum of Λ in $\bar{p}$ ^{20}Ne at rest. (b) Momentum spectrum of K_S^0 in $\bar{p}$ ^{20}Ne at rest. L cut of 1 cm. Error bars given are statistical.

Both fireballs, with $B=0$ and $B=1$, contribute to the K_S^0 production, but according to the assumption made, the Λ production is due to the $B=1$ fireball only. Since the Λ yield is 11.85% for $\bar{p}$ ^{181}Ta at 4 GeV/c [ref. [2])], $P_\Lambda > 12\%$ if $P_f < 1$. If we put $P_f = 1$ we get $R = 2.8$.

A comparison of experimental and theoretical values or R in table 8 (Λ hyperons produced only by $B=1$ fireballs) and table 7 (Λ hyperons produced only by rescattering of $\bar{K}$) indicates that the K_S^0 yield is over-estimated for annihilations in flight when $A \geq 4$. The assumption about $\Sigma^\pm \to \Lambda$ conversion will decrease P_f in table 8 and thus increase the K_S^0 yield. For instance, if we assume the fraction of $\Sigma^\pm$ produced in $B=1$ annihilations to be 5.6% [ref. [8])] and assume a $\Sigma^\pm \to \Lambda$ conversion rate of ≈ 0.5 [ref. [23])], the quoted value of $R=0.71$ in $\bar{p}$ ^{20}Ne changes to $R=0.65$ and P_f changes from 25.6% to 18.7%.

A sensitive parameter is the production rate $P_{\bar{K}K}$ of $\bar{K}K$ pairs in the nucleus and its dependence of the momentum of the antiproton. When estimating R in table 7 we have assumed a value of $P_{\bar{K}K}$ and then deduced the value of $P_{\bar{K}\to\Lambda}$. Based on the $2V^0$ events we can estimate both $P_{\bar{K}K}$ and $P_{\bar{K}\to\Lambda}$.

The number of detected $K_S^0(\Lambda)$ in $\bar{p}$ ^{4}He at rest is 325 (292). This gives a total number of produced K_S^0 of $777 = 72645 \times (1.07\%)$ and a total number of produced Λ of $813 = 72645 \times (1.12\%)$. The probability to detect a $K_S^0(\Lambda)$ is thus 0.418 (0.359). Hence, the probability to detect a $K_S^0 K_S^0$ (ΛK_S^0) pair is 0.17 (0.15). Therefore the corrected number of $K_S^0 K_S^0$ (ΛK_S^0) is 64 (206).

We now estimate $P_{\bar{K}K}$ and $P_{K\to\Lambda}$ based on the following assumptions:
- $\bar{K}K$ pairs are produced in a $B=0$ state only.
- ΛK pairs are produced by $\bar{K}$ rescattering (i.e. from $\bar{K}^0K^0$ (27%) and K^0K^- (30%)).
- We neglect charge exchange of kaons and rescatter of other produced particles ($\omega N, \ldots$).

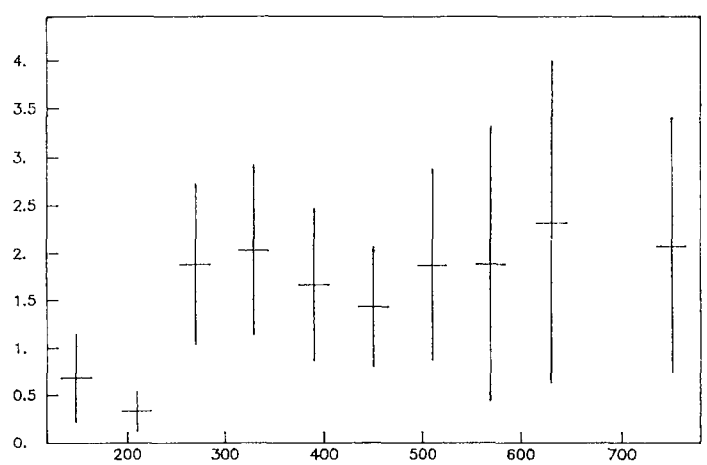

Fig. 4. Distribution of the ratio $n_{K_S^0}/n_\Lambda$ for $\bar{p}$ ^{20}Ne corrected for loss due to cut in decay length L of 1 cm. $n_{K_S^0}$ and n_Λ are the corrected numbers of K_S^0 and Λ in each bin. The spectra are normalized to each other.

The total number of antiprotons decaying at rest in ^{4}He is 72645. The probability that a $\bar{K}K$ pair contributes to a $K^0_S K^0_S$ pair is $\frac{1}{4}(0.27) = 6.75 \times 10^{-2}$ and the probability that a $\bar{K}K$ contributes to a $K^0_S \bar{K}$ pair is $\{\frac{1}{2}(0.27) + \frac{1}{2}(0.30)\} = 0.285$. Hence, the probability that a $\bar{K}K$ pair is produced, but $\bar{K}$ is not converted to a Λ is 0.013 ± 0.004 and that a $\bar{K}K$ pair is produced and $\bar{K}$ is converted to a Λ is 0.0100 ± 0.0025.

Now we can write down two equations:

$$P_{\bar{K}K}(1 - P_{\bar{K}\to\Lambda}) = 0.013 \pm 0.004 \qquad \text{(from } K^0_S K^0_S \text{ events)}$$

$$P_{\bar{K}K} P_{\bar{K}\to\Lambda} = 0.0100 \pm 0.0025 \qquad \text{(from } \Lambda K^0_S \text{ events)}$$

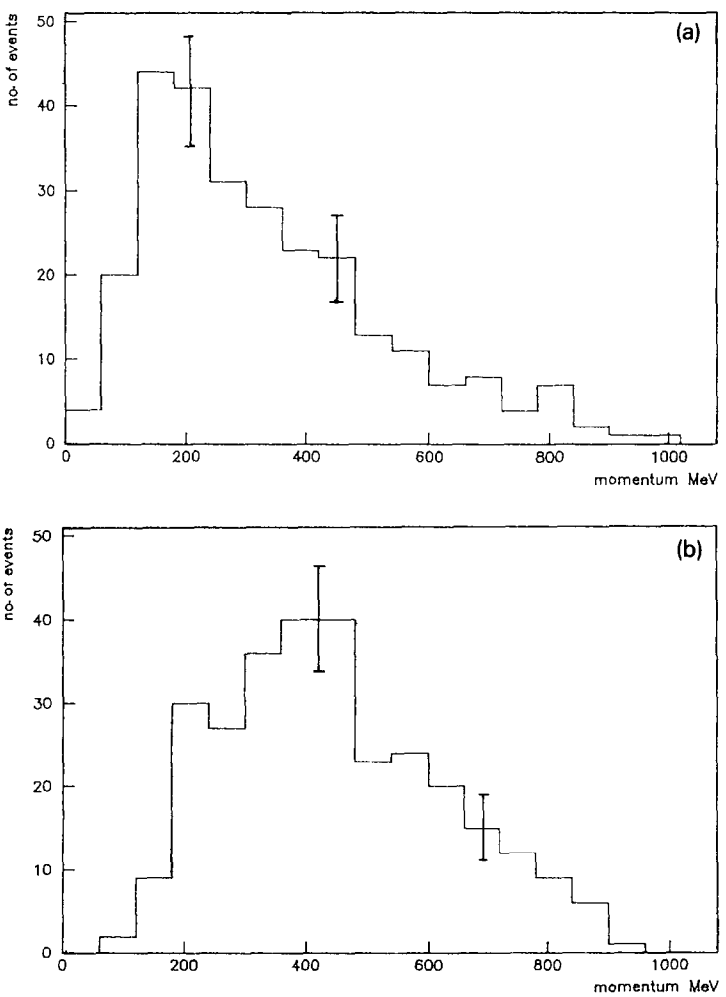

Fig. 5. (a) Momentum spectrum of Λ in $\bar{p}$ ^{4}He at rest. (b) Momentum spectrum of K^0_S in $\bar{p}$ ^{4}He at rest. L cut of 1 cm. Error bars given are statistical.

or

$$P_{\bar{K}K} = 0.023 \pm 0.005\,, \qquad P_{\bar{K}\to\Lambda} = 0.43 \pm 0.14\,.$$

These numbers are consistent with the assumption $P_{\bar{K}K} = 3\%$ made previously and with the associated value $P_{\bar{K}\to\Lambda} = 0.37$ (see table 7).

Next we make the assumptions as in table 8:

(i) ΛK_S^0 comes from decay of $B = 1$ fireballs only.

(ii) $P_{\bar{K}\to\Lambda} = 0$.

(iii) $P_\Lambda = 7.6\%$.

(iv) $\bar{K}K$ pairs are produced not only in $B = 0$, but in $B = 1$ fireballs [3.2%, ref. [8])] as well. We assume that the production of $\Lambda(\Sigma^0)K$ final states in 4 times greater than the production of $\Lambda(\Sigma^0)K_S^0$ in $B = 1$ annihilations. We can then estimate an upper limit for the probability P_f of $B = 1$ annihilations as

$$P_f = \frac{4N_{\Lambda K_S^0}}{P_\Lambda N_{\bar{p}}}$$

where $N_{\Lambda K_S^0}$ is the number of ΛK_S^0 pairs produced. We get $P_f = 0.15$, i.e. the same value as in table 8 ($\bar{p}$ ^{4}He at rest). But in order to reproduce the number of $K_S^0K_S^0$ we end up with a negative $P_{\bar{K}K}$. If we increase P_Λ to about 10% then $P_{\bar{K}K} \approx 0$ reproduces the $K_S^0K_S^0$ data.

3. Momentum spectra

3.1. EXPERIMENTAL MOMENTUM SPECTRA OF Λ, K_S^0 AND π^-

Fig. 3a, b shows the momentum spectra of Λ and K_S^0 in $\bar{p}$ ^{20}Ne, and fig. 5a, b shows the corresponding spectra in $\bar{p}$ ^{4}He, always at rest. In these spectra we have made a cut in decay length L of 1 cm. The corresponding mean values are shown in table 6 with (in parentheses) and without L cut.

The momentum spectra for these two targets are very similar when we compare the Λ spectra in ^{4}He and ^{20}Ne (fig. 7a). We observe the same thing when comparing the K_S^0 spectra (fig. 7b). However, there is a marked difference between the Λ and the K_S^0 spectra for both target masses. In figs. 4 and 6 we show the distributions of the ratio $n_{K_S^0}/n_\Lambda$ for $\bar{p}$ ^{20}Ne and $\bar{p}$ ^{4}He. $n_{K_S^0}$ and n_Λ are the numbers of K_S^0 and Λ in each bin, respectively, and are corrected for event loss due to a cut of 1 cm in the decay length.

We observe an excess of low momentum Λ compared to K_S^0. In fig. 8a, b we show the momentum distributions of Λ and K_S^0 in ^{3}He at rest. In fig. 8c the two spectra are compared. We observe a similar shift of Λ momentum compared to K_S^0 as for ^{4}He and ^{20}Ne, but not so strong.

In $\bar{p}$d annihilations the momentum spectra of π, K_S^0 and Λ are essentially the same [24]). Thus our results indicate that the nucleus modify the spectra when $A \geq 4$.

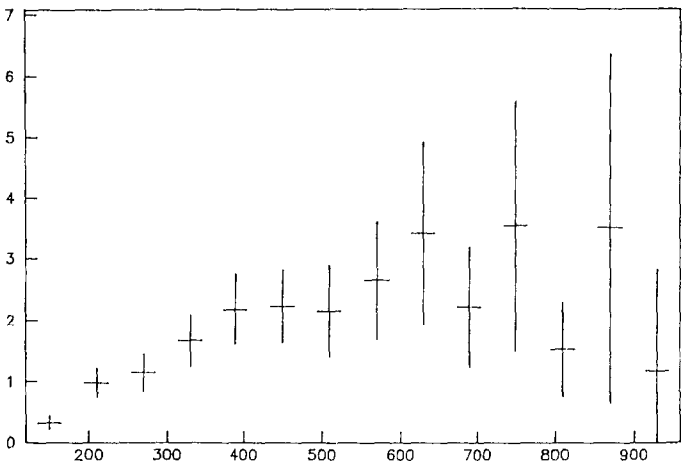

Fig. 6. Distribution of the ratio $n_{K_S^0}/n_\Lambda$ for $\bar{p}$ ^{4}He corrected for loss due to cut in decay length L of 1 cm. $n_{K_S^0}$ and n_Λ are the corrected numbers of K_S^0 and Λ in each bin. The spectra are normalized to each other.

In order to investigate further the dependence of the momentum distribution on the target mass we have measured the momenta of π^- produced in ordinary annihilations (all types) at rest and at 607 MeV/c in ^{20}Ne and ^{4}He. In fig. 9 we compare the distributions from the two targets at rest, including only events with a dip angle less than 30° (absolute value). For the momentum mean values, see table 6.

In fig. 10 we do the same thing at 607 MeV/c, including only events with an azimuth angle less than 45° (absolute value, in a plane normal to the beam. An azimuth of 0° is approximately along the z axis, and the beam is approximately in the xy plane).

We observe a shift in momentum due to different target masses: the Ne spectrum is less energetic than the He one. It is reasonable to ascribe this difference to the copious production of Δ resonances. Within statistics we see no such mass effects in the Λ and K_S^0 momentum distributions. Note that the π^- momentum spectra are more similar to the Λ spectra than the K_S^0 spectra are (fig. 11a, 11b). In these figures there is no cut in the decay lengths, neither for the Λ nor for the K_S^0. Mean numbers of charged particles $\langle N_{ch} \rangle$ and negative particles $\langle N_- \rangle$ for different target masses are shown in table 6.

3.2. AN ANALYSIS OF THE DATA BASED ON SIMPLE ASSUMPTIONS

It may be useful to see if the predictions of simple models may reproduce our data at rest and at 607 MeV/c. We have used a simulation model where the nucleus is considered to be a continuous medium with a nuclear density given by Woods-Saxon [25]). We subdivide the nucleus in cells and follow the particle through the

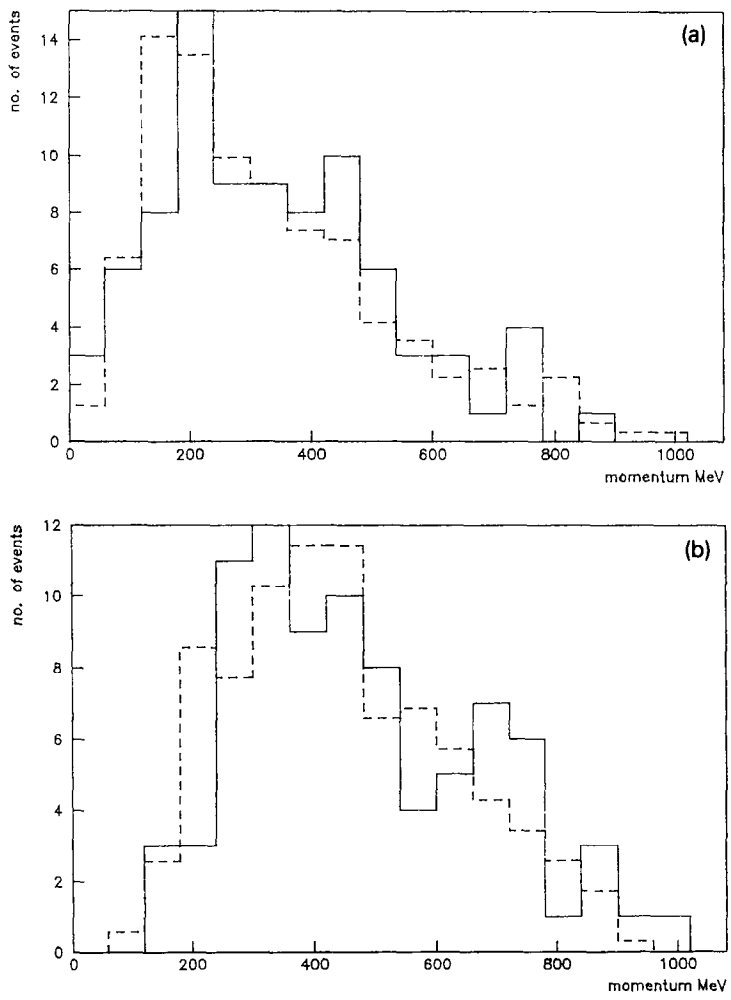

Fig. 7. (a) Momentum spectrum of Λ in $\bar{p}$ ^{4}He and $\bar{p}$ ^{20}Ne at rest. (b) Momentum spectrum of K^0_S in $\bar{p}$ ^{4}He and $\bar{p}$ ^{20}Ne at rest. L cut of 1 cm. Solid line: $\bar{p}$ ^{20}Ne; dashed line: $\bar{p}$ ^{4}He.

nucleus investigating whether the particle interacts in each cell. Here we base the interaction probability on the particle's mean free path. The distribution of antiproton annihilations points in the nucleus depends of whether we consider annihilations at rest or in flight.

(a) We assume the path of the antiproton to be straight lines. We further assume the target nucleons to be at rest, and we neglect all kinds of interaction before the annihilation takes place.

(b) At rest we use a formula for radial absorption probability taken from Iljinov *et al.* [26]).

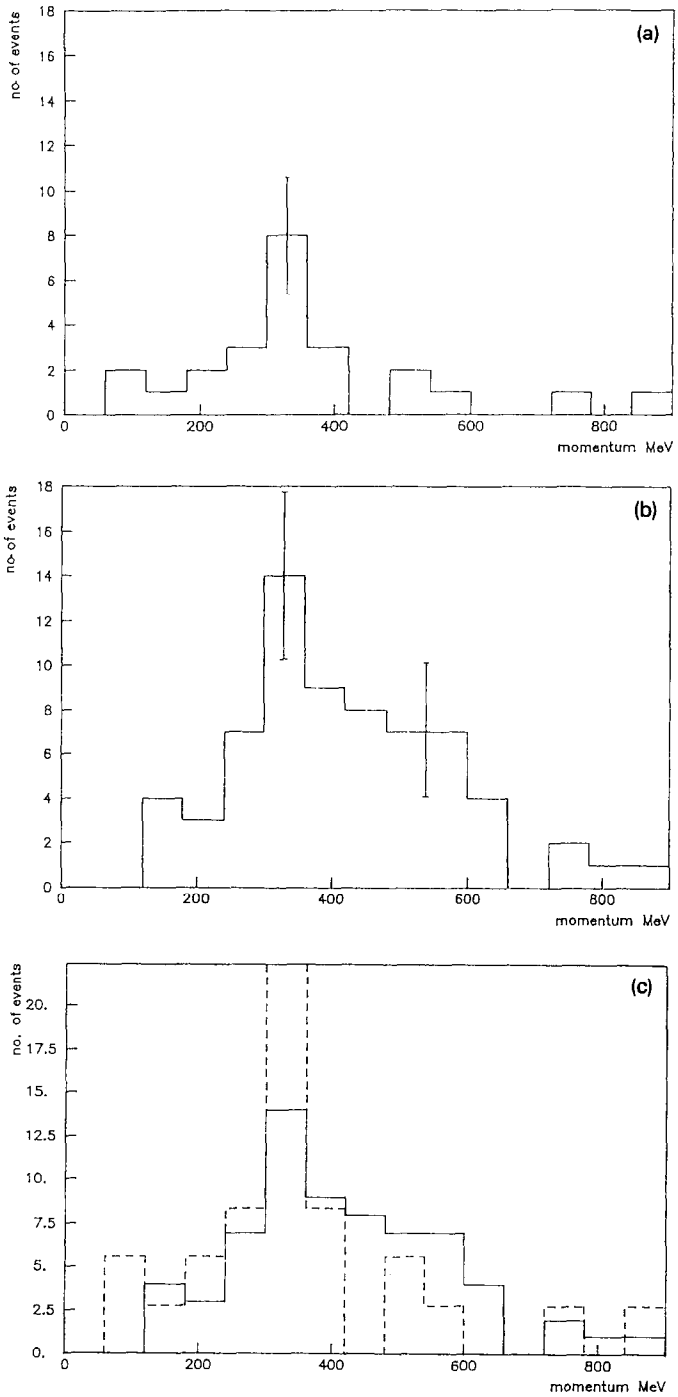

Fig. 8. (a) Momentum spectrum of Λ in $\bar{p}$ ^{3}He at rest. (b) Momentum spectrum of K^0_S in $\bar{p}$ ^{3}He at rest. L cut of 1 cm. Error bars given are statistical. (c) Momentum spectrum of Λ and K^0_S in $\bar{p}$ ^{3}He at rest. L cut of 1 cm. Solid line: K^0_S; dashed line: Λ.

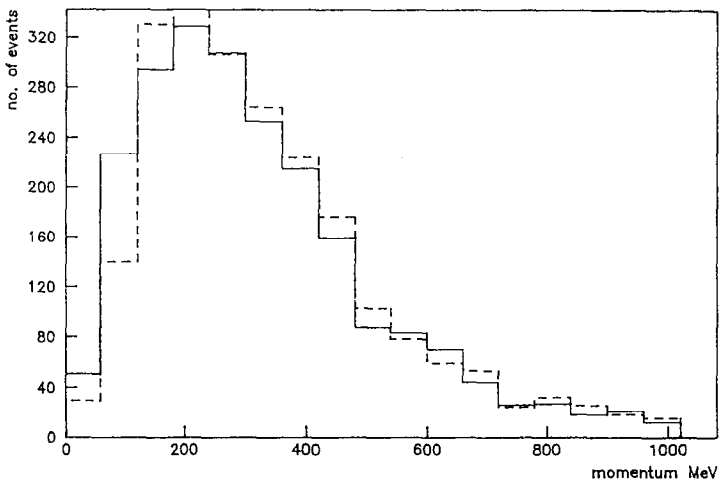

Fig. 9. Momentum spectrum of π^- in $\bar{p}$ ^{4}He and $\bar{p}$ ^{20}Ne at rest, ordinary annihilations. Dip cut $<|30°|$. Solid line: $\bar{p}$ ^{20}Ne; dashed line: $\bar{p}$ ^{4}He.

(c) In flight we choose the impact parameter at random according to an isotropic distribution in a plane normal to the beam. The experimental annihilation cross section taken to be [3])

$$\sigma_{\bar{p}} = 44/\beta \text{ mb},$$

where β is the velocity of the antiproton. At the point of $\bar{p}$ annihilation we assume $B = 0$ fireballs to be produced in a way described by Cugnon *et al.* [3]). We assume the target nucleons to be at rest.

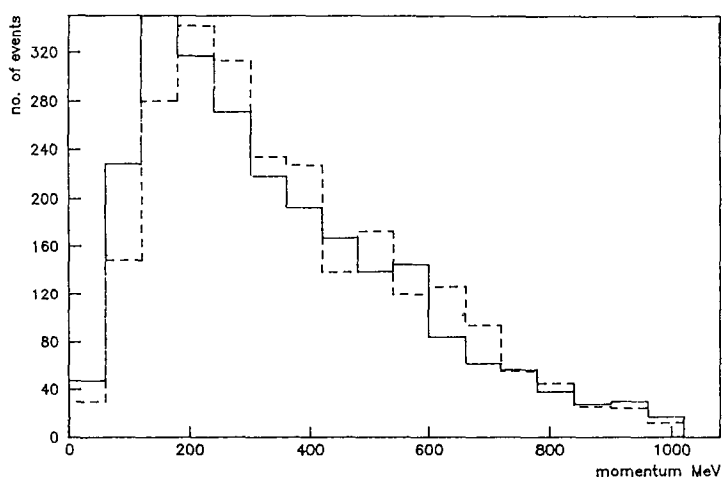

Fig. 10. Momentum spectrum of π^- in $\bar{p}$ ^{4}He and $\bar{p}$ ^{20}Ne at 607 MeV/c, ordinary annihilations. Azimuth (ϕ) cut $<|45°|$ (see text). Solid line: $\bar{p}$ ^{20}Ne; dashed line: $\bar{p}$ ^{4}He.

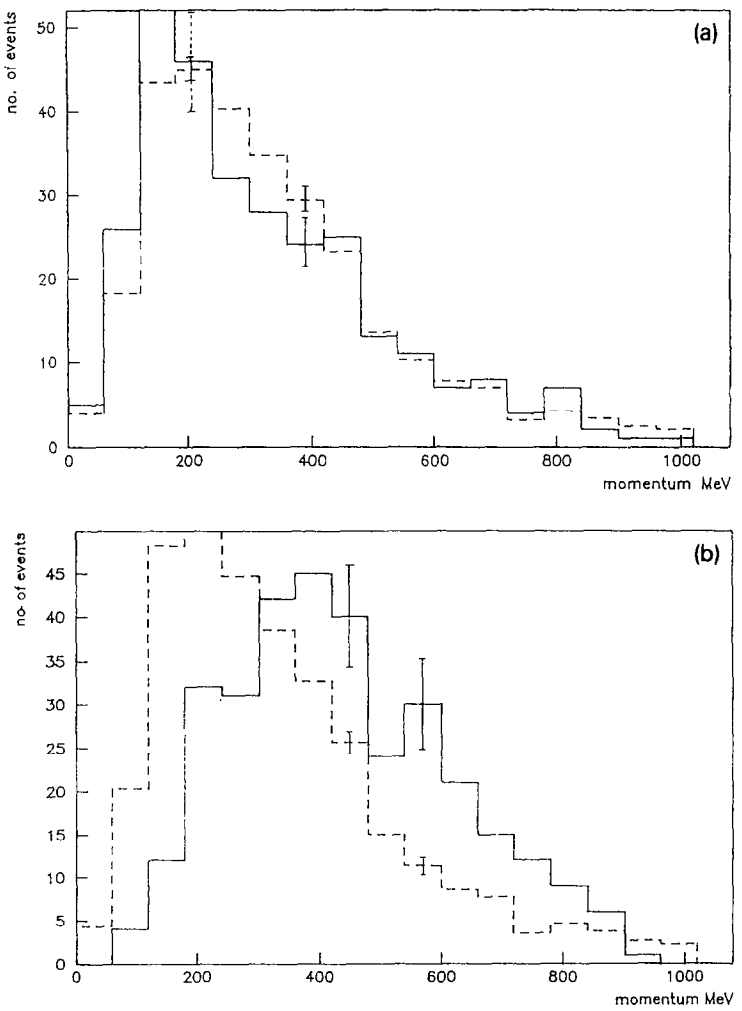

Fig. 11. (a) Momentum spectrum of Λ compared to π^- from ordinary annihilations in $\bar{p}$ ^{4}He at rest. Solid line: Λ (no L cut); dashed line: π^-. (b) Momentum spectrum of K^0_S compared to π^- from ordinary annihilations in $\bar{p}$ ^{4}He at rest. Solid line: K^0_S (no L cut); dashed line: π^-. Error bars given are statistical.

After some time the fireballs will either decay into a $\bar{K}K(m\pi)$ state, i.e.

$$\bar{p}N \to \bar{K}K(m\pi), \qquad m = 0, 1 \ldots,$$

or absorb another nucleon to produce a $B = 1$ final state, i.e.:

$$\to YK(m\pi), \qquad m = 0, 1 \ldots, \qquad \text{where } Y = \Lambda, \Sigma$$

$$\to N\bar{K}K(m\pi), \qquad m = 0, 1 \ldots,$$

$$\to \Xi KK(m\pi), \qquad m = 0, 1 \ldots,$$

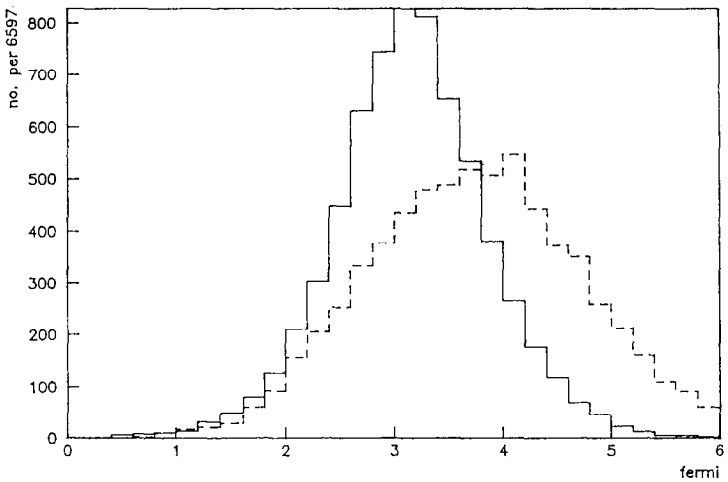

Fig. 12. Distribution of anninilation radial distance in ^{20}Ne. Solid line: at 607 MeV/c; dashed line: at rest.

The lifetime τ_{fb} and the absorption cross section σ_{fb} of the fire ball are taken to be [2]:

$$\tau_{fb} = 1 \text{ fm}/c, \qquad \sigma_{fb} = 44/\beta_{fb}$$

where β_{fb} is the velocity of the fireball.

We consider now two alternatives which we shall call model I and model II.

(a) Model I. Here we consider the $B = 0$ $\bar{K}K(m\pi)$ state only.

In annihilations at rest we assume that the $\bar{K}K$ $(m\pi)$ system is created at the same points as the annihilations of antiprotons have taken place. At these points

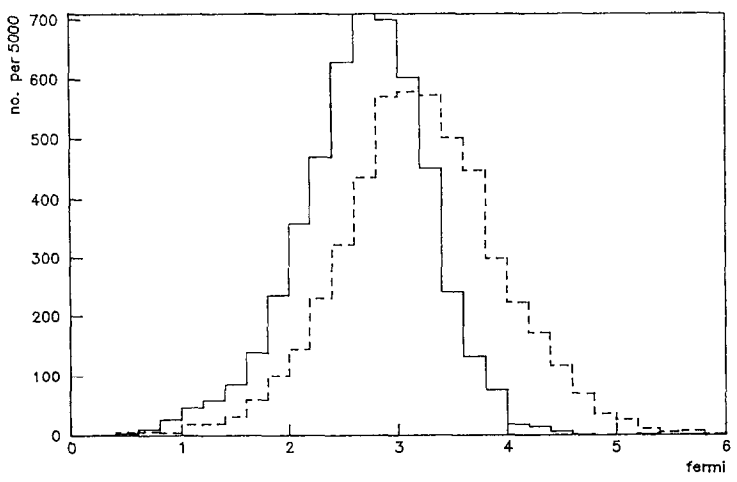

Fig. 13. Distribution of fireball radial distance in ^{20}Ne at 607 MeV/c. Solid line: $B = 1$ fireballs; dashed line: $B = 0$ fireballs.

we produce the $\bar{K}K(m\pi)$ system according to phase space using the program FOWL. $K(\bar{K})$ are emitted isotropically. The weighting procedure of the different channels is taken from ref. [3]).

In flight we produce $\bar{K}K(m\pi)$ in the center of mass of the $B=0$ fireball and according to phase space. From the decay points of the $B=0$ fireballs $K(\bar{K})$ are emitted isotropically.

In this model I we assume that Λ hyperons are produced through rescattering of $\bar{K}$ only i.e.:

$$\bar{K}N \rightarrow YX\,, \qquad \text{where } Y=\Lambda, \Sigma^0$$

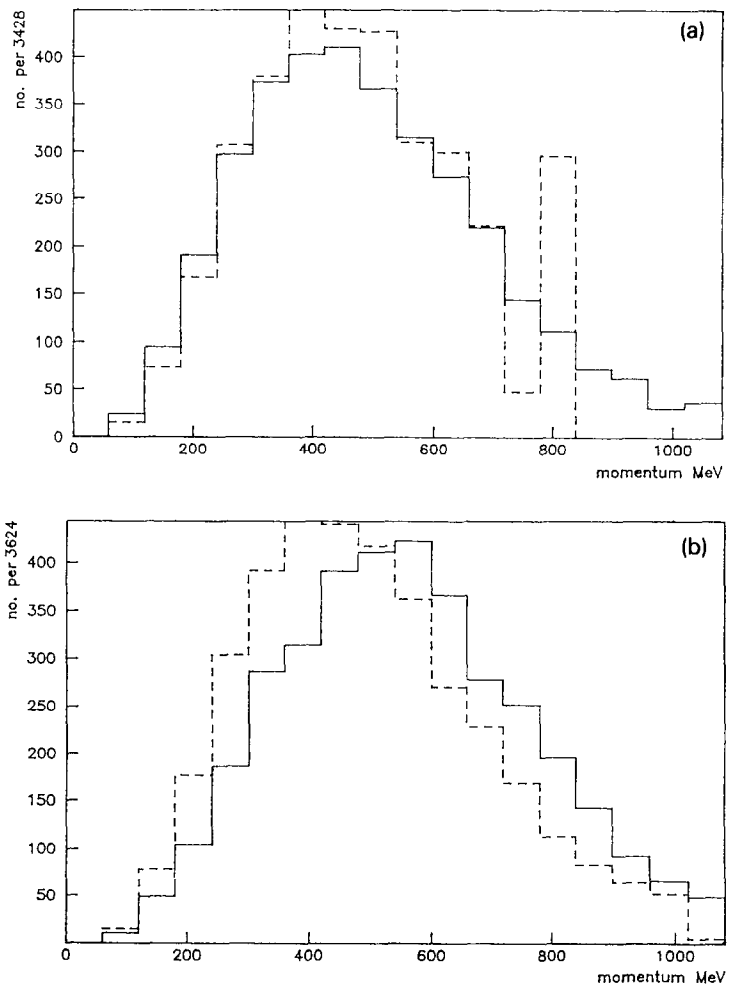

Fig. 14. Momentum spectrum of Λ and K^0_S in $\bar{p}$ ^{20}Ne at rest from (a) model I, (b) model II, assumption A. L cut of 1 cm. Solid line: Λ; dashed line: K^0_S.

neglecting contributions from $\Sigma^{\pm}$, ω (although we will introduce the $\Sigma^{\pm} \to \Lambda$ conversion later on).

The average absorption cross section of $\bar{K}$ is taken to be 24 mb. This has been obtained by averaging the experimental cross section (on nucleons) over momentum, using phase space.

We can now generate the Λ momentum spectrum, assuming that

$$\bar{K}N \to \Lambda\pi$$

i.e. a two-body final state only.

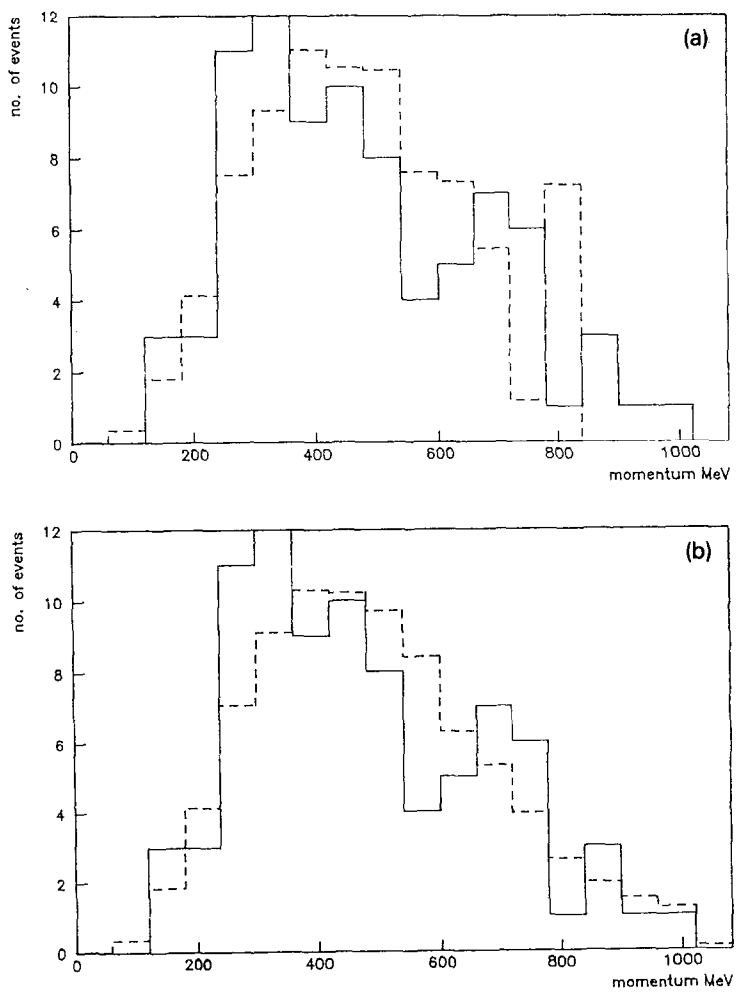

Fig. 15. Momentum spectrum of K_S^0 from (a) model I, (b) model II, assumption A in $\bar{p}$ ^{20}Ne at rest. L cut of 1 cm. Solid line: experiment; dashed line: model.

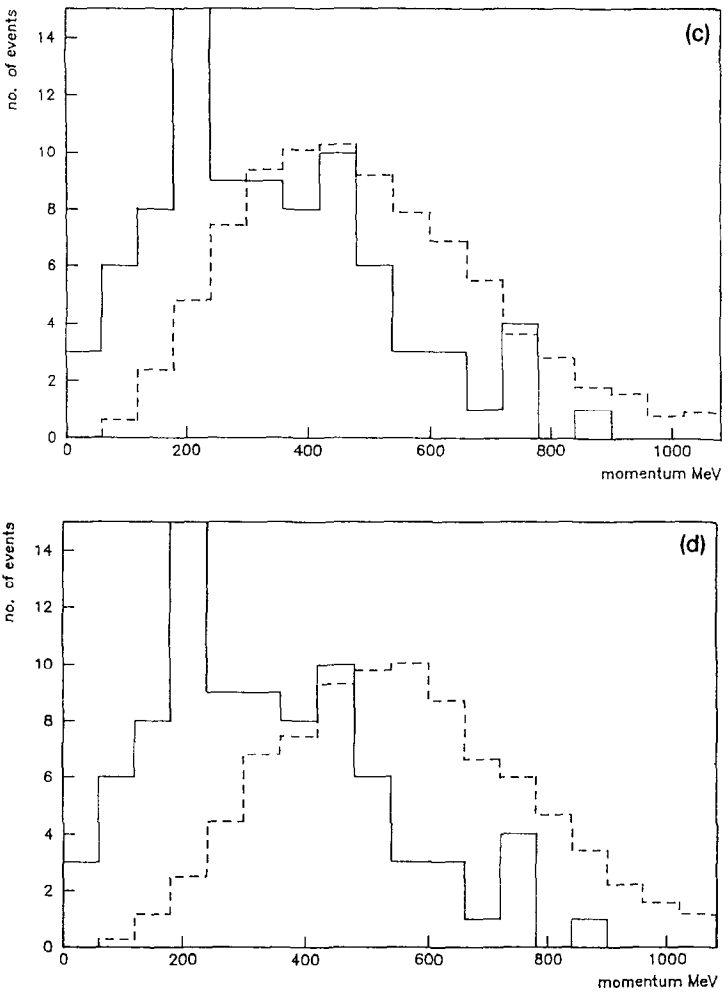

Fig. 15 (continued). Momentum spectrum of Λ from (c) model I, (d) model II, assumption A in $\bar{p}$ ^{20}Ne at rest. L cut of 1 cm. Solid line: experiment; dashed line: model.

In the center-of-mass system of the $\Lambda\pi$ the Λ is emitted isotropically.

(b) Model II. Here we consider the final states produced by the $B = 1$ fireballs introduced above, i.e. we assume that Λ hyperons are produced by $B = 1$ fireballs only.

At rest we assume that the particles in different channels are produced at the same points as taken place the annihilations of antiproton. From these points we produce the different channels according to phase space. Λ(K) are emitted isotropically.

In flight we consider only the case where the fireball decays to $B = 1$ final states. From these points, and in the center of mass of the fireball, we produce the different channels according to phase space. Λ(K) are emitted isotropically in this system.

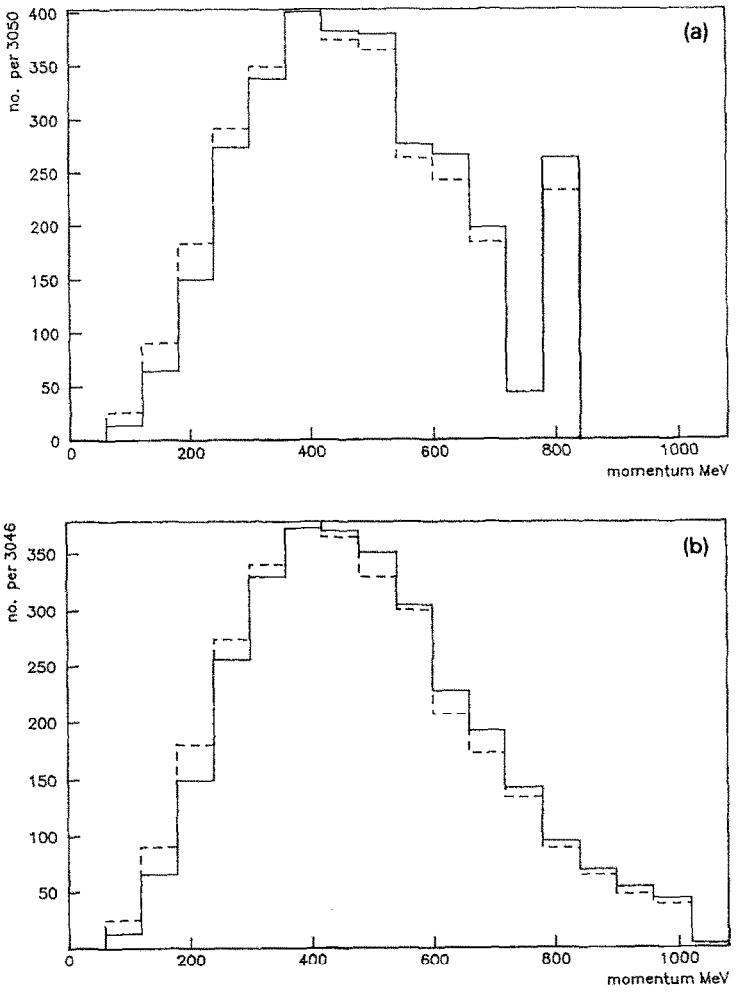

Fig. 16. Momentum spectrum of K_S^0 for (a) model I, (b) model II, assumption A and B in $\bar{p}$ ^{20}Ne at rest. L cut of 1 cm. Solid line: assumption A; dashed line: assumption B.

Finally we make a Lorentz transformation back to the lab system. We can now generate the Λ momentum spectrum assuming that the Λ is produced in

$$\bar{p}(2N) \to \Lambda(m\pi), \qquad m = 0, 1, \ldots .$$

Likewise the K_S^0 momentum spectrum is generated assuming that the K_S^0 is produced in

$$\begin{aligned} \bar{p}(2N) &\to \Lambda K(m\pi) \\ &\quad \Sigma K(m\pi) \\ &\quad N\bar{K}K(m\pi) \\ &\quad \Xi KK(m\pi), \qquad m = 0, 1, \ldots . \end{aligned}$$

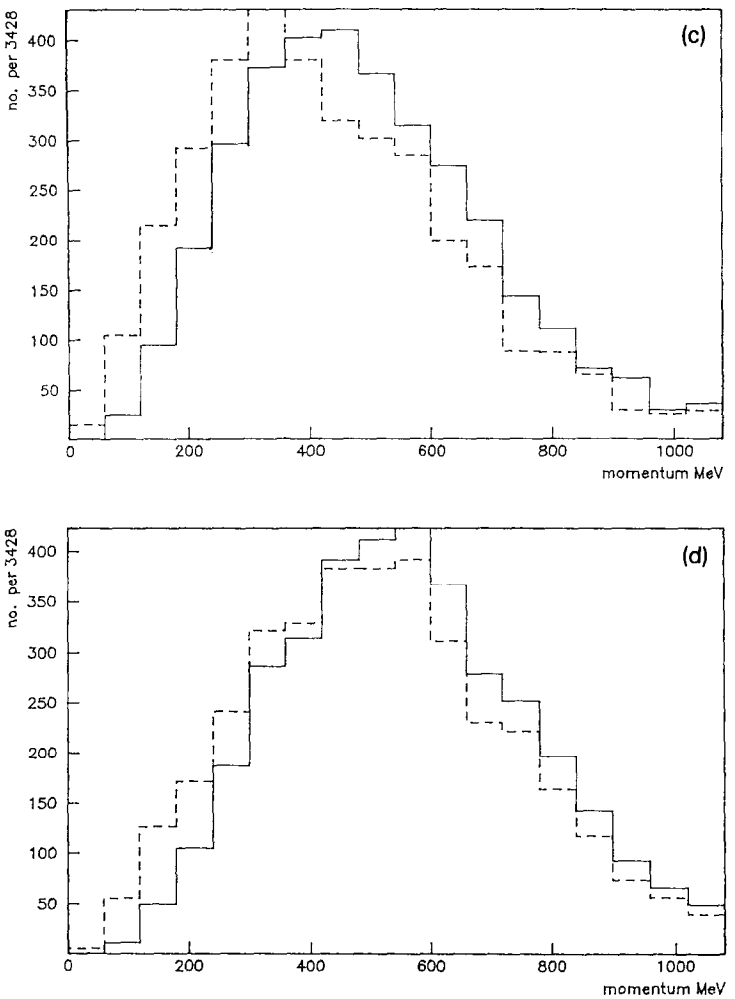

Fig. 16. (continued). Momentum spectrum of Λ for (c) model I, (d) model II, assumption A and B in $\bar{p}$ ^{20}Ne at rest. L cut of 1 cm. Solid line: assumption A; dashed line: assumption B.

The weighting of different channels is made according to ref. [3]).

Finally we introduce two mutually excluding assumptions (A) and (B) about the influence of the nucleus on the produced strange particles.

(A) We neglect all kinds of interactions of the produced strange particles with the nucleus (except $\bar{K}$ absorption in model I).

(B) We introduce a certain number of final-state interactions of the produced strange particles in order to investigate such effects on the momentum spectra. This assumption will only be applied to $\bar{p}$ Ne annihilations, where we assume

(i) $\bar{K}^0$ can scatter elastically with $(\sigma_{\bar{K}^0})_{el} = 27$ mb and be absorbed with $(\sigma_{\bar{K}^0})_{abs} = 24$ mb [ref. [27])],

(ii) K^0 can scatter elastically with $(\sigma_{K^0})_{el} = 10$ mb [ref. [27])],

(iii) Λ can scatter elastically with $(\sigma_\Lambda)_{el} = 27$ mb [ref. [28])], where the cross sections are averaged over momenta.

3.2.1. Penetration depth in $\bar{p}$ ^{20}Ne at rest and at 607 MeV/c. Point (c) in subsect. 2.3.2 seems to reflect the fact that $\bar{p}$ penetrates deeper into the nucleus than at rest [19,29]). We have calculated the distributions of annihilation points in ^{20}Ne at 607 MeV/c and at rest using model I.

The results are shown in fig. 12, and the penetration effect is clearly demonstrated. In fig. 13 we show the decay points of $B = 0$ and $B = 1$ fireballs in ^{20}Ne at 607 MeV/c. Following each produced $\bar{K}$ from a $B = 0$ fireball through the nucleus we can give an estimate of the absorption probability of $\bar{K}$ in ^{20}Ne. We find this to be 0.27 at

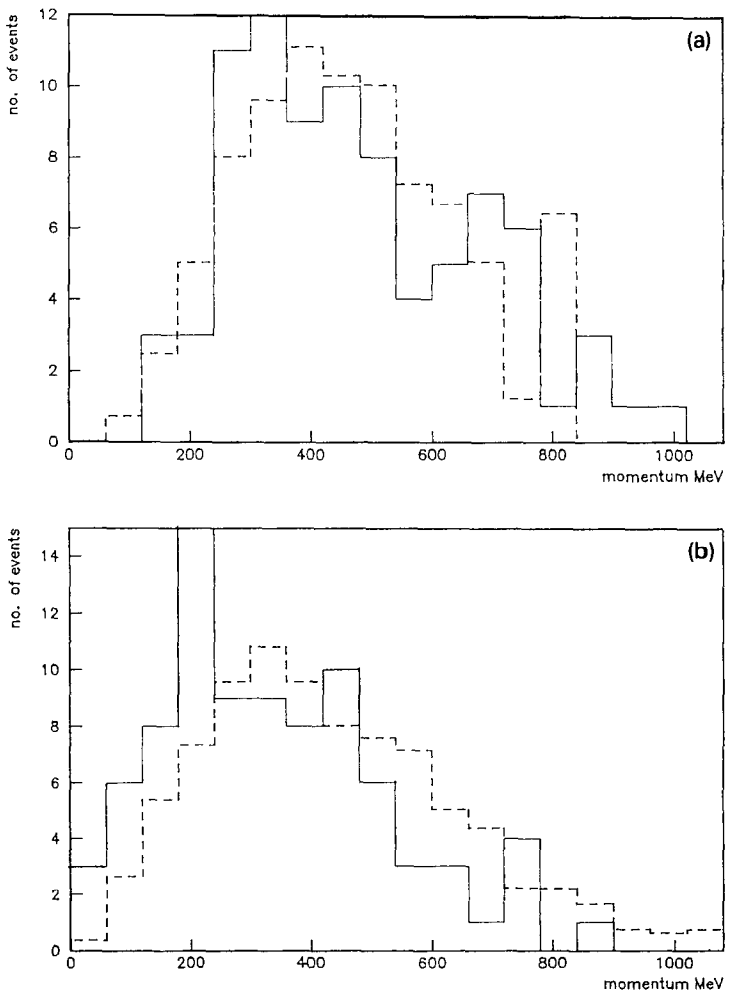

Fig. 17. Experimental momentum spectrum of (a) K^0_S (b) Λ in $\bar{p}$ ^{20}Ne at rest with the predictions of model I assumption B). L cut of 1 cm. Solid line: experiment; dashed line: model.

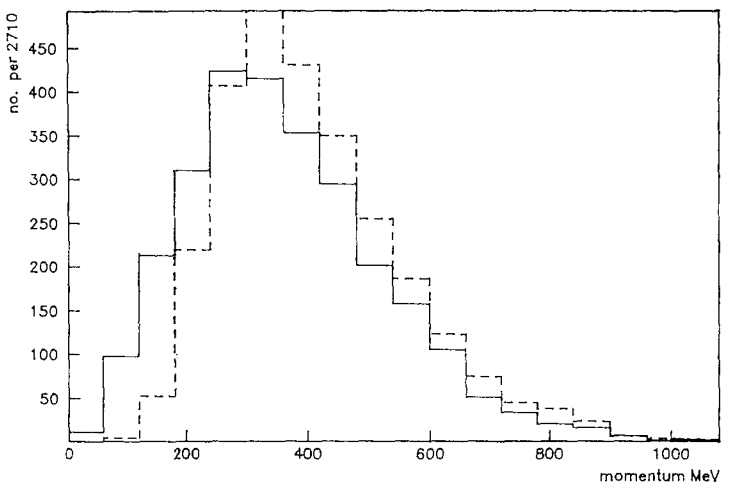

Fig. 18. Momentum spectrum of Λ from model I with $\Sigma \to \Lambda$ conversion in $\bar{p}$ ^{20}Ne at rest. $(\sigma_\Lambda)_{el} = 0$ and 27 mb, respectively. L cut of 1 cm. Solid line: $(\sigma_\Lambda)_{el} = 27$ mb; dashed line: $(\sigma_\Lambda)_{el} = 0$ mb.

rest and 0.40 at 607 MeV/c. (Note that these are the same values as given in table 7 for $P_{\bar{K} \to \Lambda}$.) In making this calculation we have kept the absorption cross section of $\bar{K}$ constant (this cross section decreases with energy [6]), but for these calculations the effect is small).

This increase in the absorption probability of $\bar{K}$ is due only to different distributions of decay points of the $B = 0$ fireballs in the nucleus and to different $\bar{K}$ angular distribution in the lab system. An increase with energy of the production of $\bar{K}K$ pairs increases also both the Λ and the K_S^0 yield. At constant energy, but with increasing A the nuclear effect is the dominant one and may explain the fact that R_Λ increases and $R_{K_S^0}$ decreases as a function of A for antiproton annihilations below 1600 MeV/c. Our estimate of the $B = 1$ production rate is 0.25 at 607 MeV/c, very similar to the one obtained in ref. [8]).

3.2.2. Comparisons of model generated and experimental spectra. All distributions predicted by models are weighted according to a decay length cut of $L < 1$ cm unless otherwise stated.

(a) Comparisons between model I and model II using assumption A. In fig. 14a we compare momentum spectra of Λ and K_S^0 in $\bar{p}$ ^{20}Ne at rest, using model I. The peak about 790 MeV is due to the contribution of $\bar{K}K$ channel. Apart from the tail in the Λ distribution the two spectra are similar. Model II gives different spectra, but they change in the wrong direction compared to the data (fig. 14b).

(b) Model I and II assumption A compared to data. In fig. 15a, b we compare the generated momentum spectra of K_S^0 with the experimental ones for $\bar{p}$ ^{20}Ne at rest. The agreement is reasonable both for model I and model II. Correspondingly, in fig. 15c, d we compare the Λ spectra. Neither of the models are able to reproduce the excess of low momentum events.

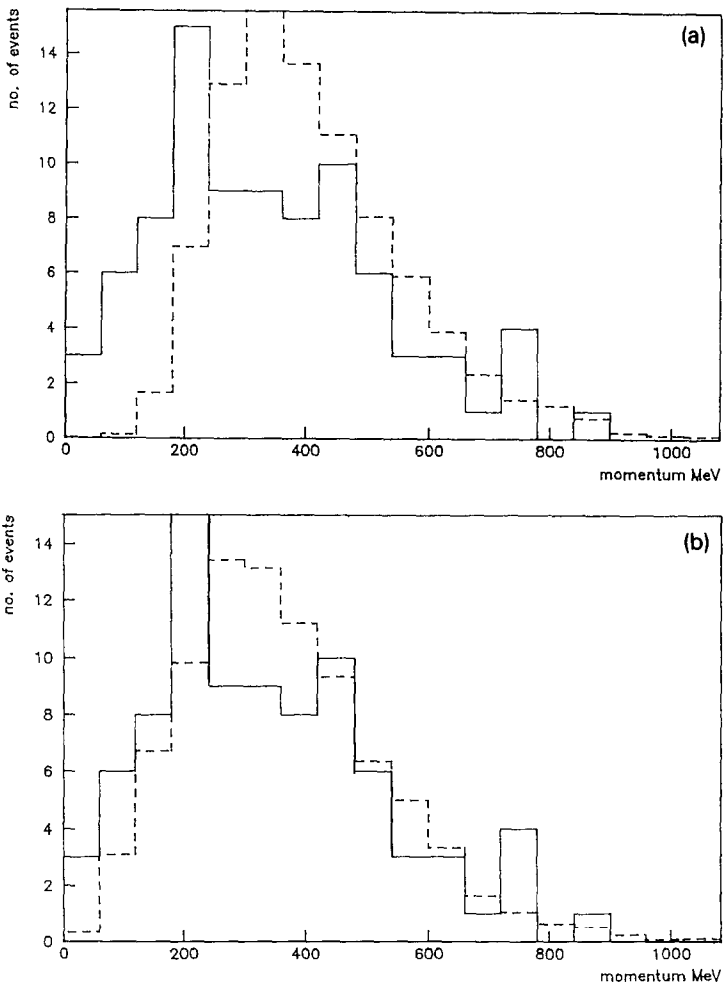

Fig. 19. Experimental momentum spectrum of Λ in $\bar{p}$ ^{20}Ne at rest compared to prediction of model I with $\Sigma \to \Lambda$ conversion. (a) $(\sigma_\Lambda)_{el} = 0$ mb. (b) $(\sigma_\Lambda)_{el} = 27$ mb. L cut of 1 cm. Solid line: Experiment; dashed line: model.

(c) Comparison of assumptions A and B. Fig. 16a contains the momentum spectra of K^0_S for model I, comparing the outcome of assumptions A and B respectively. In fig. 16b the same thing is done for model II.

The K^0_S momentum spectra are rather insensitive to assumptions A or B or to the use of model I or model II except the tail in model II.

In fig. 16c and 16d we compare the momentum spectra of Λ in the same way. Assumption B has a strong effect on the spectra (the effect is stronger when comparing spectra with no cut in L) and model I gives the best agreement with data. In fig. 17a, b we compare the experimental momentum spectra of K^0_S and Λ in $\bar{p}$ ^{20}Ne with the predictions of model I assumption B. From fig. 17b we see that there is still

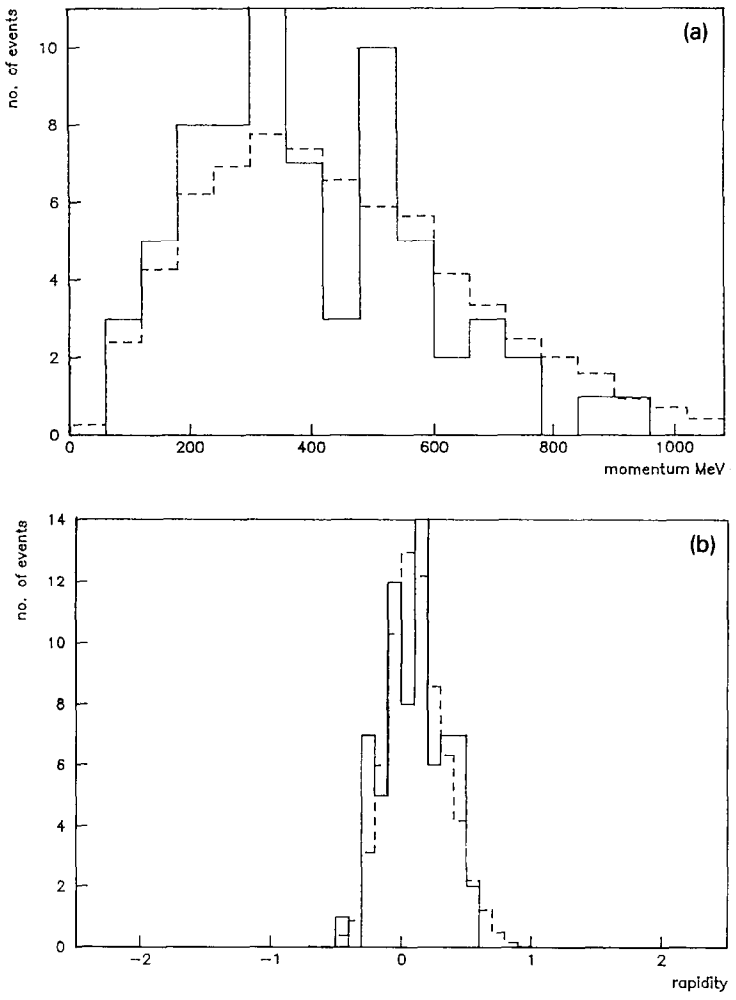

Fig. 20. (a) Experimental momentum spectrum, (b) experimental rapidity distribution, of Λ in $\bar{p}$ ^{20}Ne at 607 MeV/c compared to prediction of model I, assumption B. L cut of 1 cm. Solid line: experiment; dashed line: model.

experimentally an excess of Λ with low momentum compared to the outcome of the model. Thus it is interesting to see how the Λ spectra are influenced when we introduce $\Sigma \to \Lambda$ conversion. We expect this conversion to lower the Λ momenta on average.

(d) $\Sigma \to \Lambda$ conversion. In model I we have assumed that Λ is produced by $\bar{K}$ rescattering

$$\bar{K}N \to \Lambda\pi .$$

However, we have also the possibility that Λ is produced in a two step process

$$\bar{K} \to \Sigma \to \Lambda \qquad [\text{refs.}\ ^{6,23})] .$$

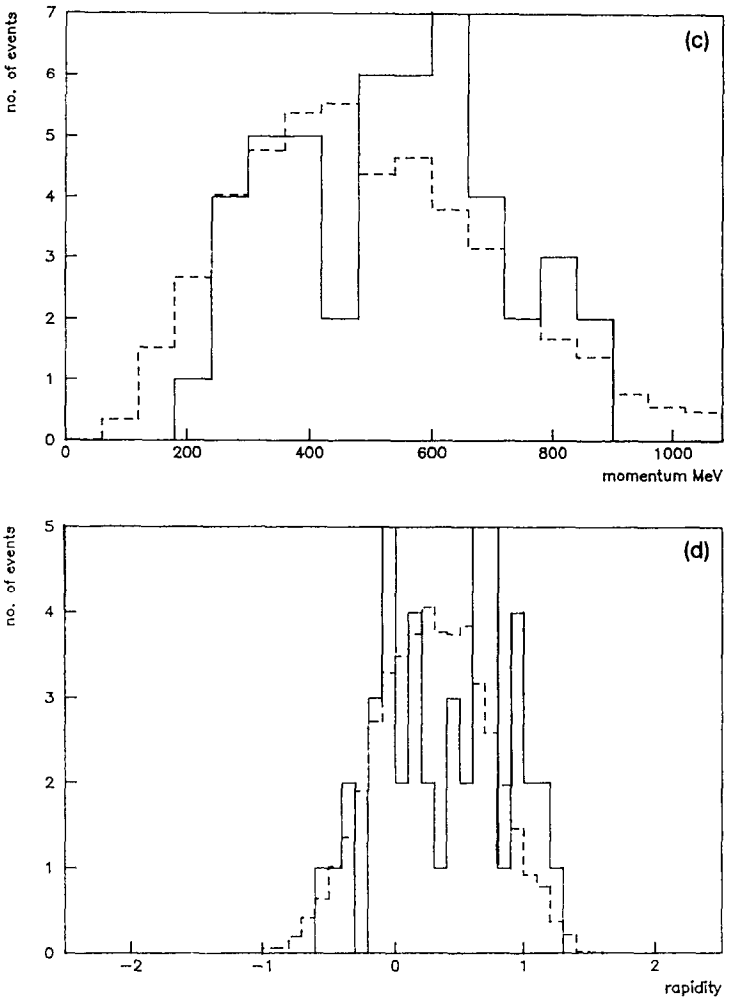

Fig. 20 (continued). (c) Experimental momentum spectrum, (d) experimental rapidity distribution of K^0_S in $\bar{p}$ ^{20}Ne at 607 MeV/c compared to prediction of model I, assumption B. L cut of 1 cm. Solid line: experiment; dashed line: model.

In order to see the influence of $\Sigma \to \Lambda$ conversion on the Λ momentum spectrum in $\bar{p}$ ^{20}Ne at rest we make the following assumption:
$\bar{K}$ produced in a $B = 0$ fireball can rescatter to give

$$\bar{K}N \to \Sigma\pi, \qquad \text{where } \Sigma N \to \Lambda N .$$

The cross section of the Σ-nucleon absorption is taken from ref. [6]). We assume that the Σ's are emitted isotropically in the $\Sigma\pi$ center-of-mass system.

In fig. 18 we compare the momentum spectra of Λ when $(\sigma_\Lambda)_{el}$ is 0 and 27 mb, respectively. In fig. 19a, b we compare with the experimental Λ momentum spectrum

in $\bar{p}$ ^{20}Ne at rest and we conclude that we get the best agreement with data when $(\sigma_\Lambda)_{el} = 27$ mb.

(e) $\bar{p}$ ^{20}Ne at 607 MeV/c. We can do similar calculations for $\bar{p}$ ^{20}Ne at 607 MeV/c. In this case we compare the experimental momentum and rapidity distributions in $\bar{p}$ ^{20}Ne at 607 MeV/c with spectra using model I and assumption B. The results are shown in fig. 20a-d. In fig. 21 we compare the momentum spectra of K^0_S with model I, assumption A, which is better than assumption B. In fig. 22a-c the momentum spectra and rapidity of Λ, when $\Sigma \to \Lambda$ conversion is assumed, are compared to the experimental distribution. The agreement is improved when we introduce the $\Sigma \to \Lambda$ conversion. This was also the case at rest. We see that it is possible to reproduce the data rather well in spite of the simplicity of the model.

(f) $\bar{p}$ ^{4}He at rest. For $\bar{p}$ ^{4}He at rest we cannot use the picture of the nucleus as a continuous medium, but we can compare the experimental data to the predictions of model I combined with assumption A where we simply assumed that $\bar{K} \to \Lambda$ at the annihilation point. Therefore any influence of the nucleus is neglected.

In fig. 23a, b we compare the experimental momentum spectra of K^0_S and Λ with the predictions of model I with assumption A. The Λ spectrum is not well reproduced. For K^0_S, however, the model reproduces the momentum spectrum fairly well. For the Λ spectrum we need some kind of modifications as we did for $\bar{p}$ ^{20}Ne at rest.

(g) $\bar{p}$ ^{3}He at rest. In fig. 24a, b we compare the experimental spectra of K^0_S and Λ with the predictions of model I with assumption A. Also here we observe an excess of Λ with too low momenta compared to model predictions.

4. Conclusions

We have reported new data on strange-particle production in antiproton nucleus annihilations at rest, using a streamer chamber, with ^{3}He, ^{4}He and ^{20}Ne as gas

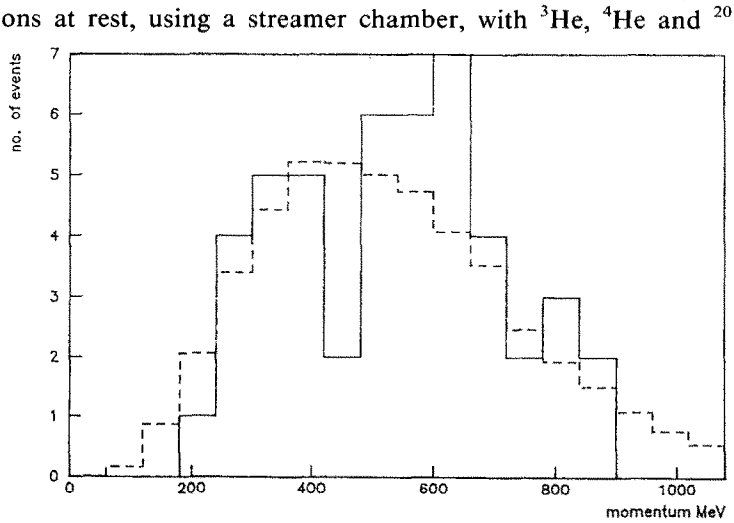

Fig. 21. Experimental momentum spectrum of K^0_S in $\bar{p}$ ^{20}Ne at 607 MeV/c compared to prediction of model I, assumption A. L cut of 1 cm. Solid line: experiment; dashed line: model.

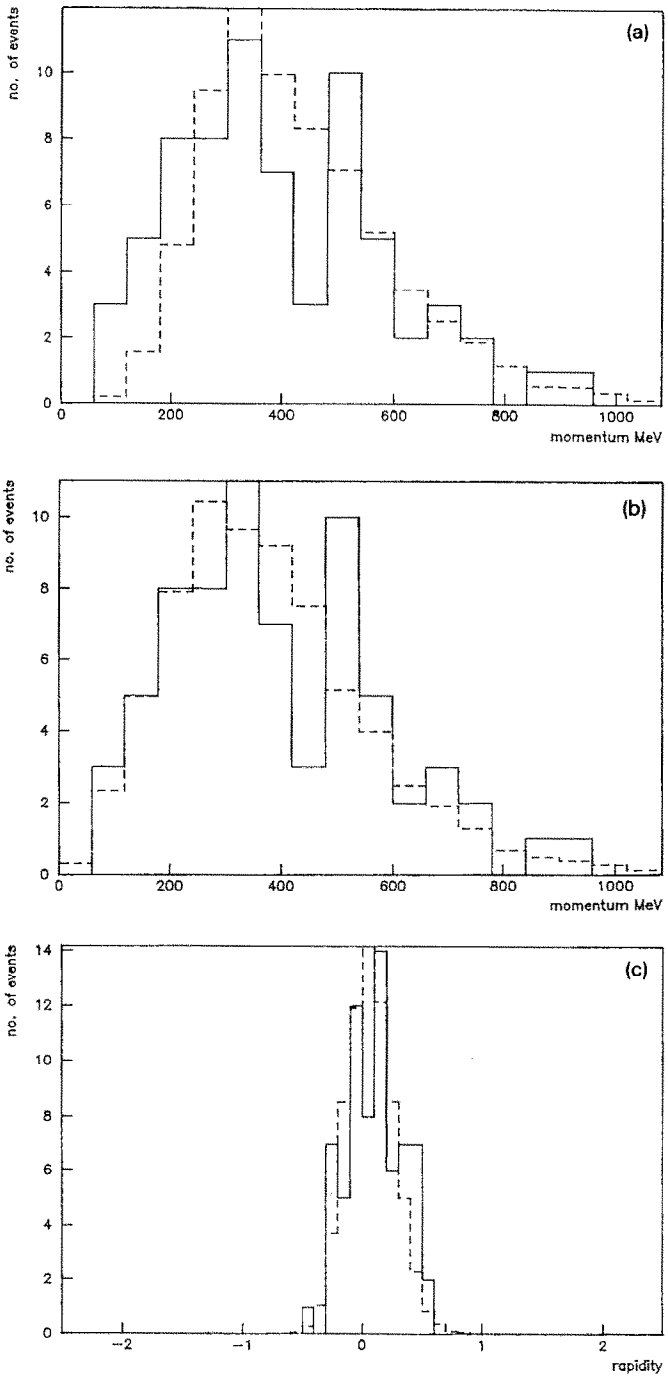

Fig. 22. Experimental momentum spectrum of Λ in $\bar{p}$ ^{20}Ne at 607 MeV/c compared to prediction of model I with $\Sigma \to \Lambda$ conversion. (a) $(\sigma_\Lambda)_{el} = 0$ mb. (b) $(\sigma_\Lambda)_{el} = 27$ mb. L cut of 1 cm. Solid line: experiment, Dashed line: model. (c) Experimental rapidity distribution of Λ in $\bar{p}$ ^{20}Ne at 607 MeV/c compared to prediction of model I with $\Sigma \to \Lambda$ conversion. $(\sigma_\Lambda)_{el} = 27$ mb. L cut of 1 cm. Solid line: experiment; dashed line: model.

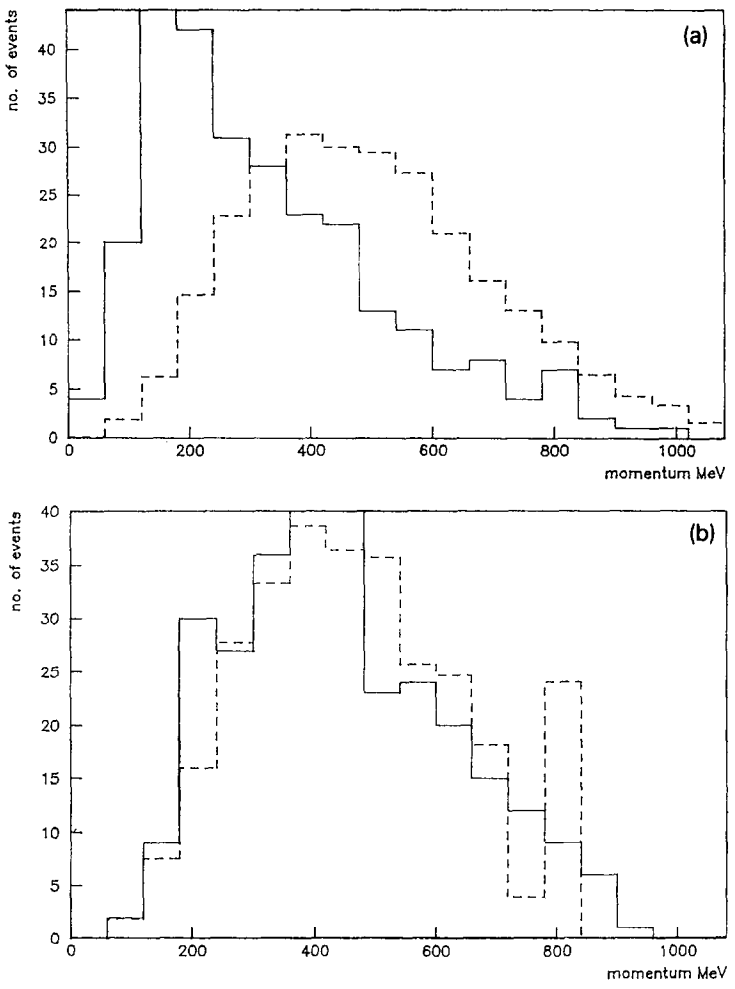

Fig. 23. Experimental momentum spectrum of (a) Λ, (b) K^0_S, in $\bar{p}$ ^{4}He at rest compared to predictions of model I assumption A. L cut of 1 cm. Solid line: experiment; dashed line: model.

targets. The data include Λ, K^0_S, ΛK^0_S and $K^0_S K^0_S$ pair production rates, momentum spectra and mean numbers of charged particles $\langle N_{ch} \rangle$ and negative particles $\langle N_- \rangle$ for different reaction channels. A complete review of $\bar{p}$-nucleus and $\bar{p}$-nucleon data at rest and in flight are given. If we compare the data at rest and at 600 MeV/c they show a dependence on target mass and antiproton momentum as follows: R_Λ increases remarkably with target mass up to $A=4$. For $A>4$ R_Λ depends weakly on A. R_Λ increases moderately with momentum. $R_{K^0_S}$ decreases with A and increases with momentum. Consequently we find a strong increase in the ratio $R = R_\Lambda / R_{K^0_S}$ up to $A=4$, and it depends weakly on A when $A>4$.

The mean numbers of negative particles $\langle N_- \rangle$ produced in non-strange final states depend on A, these numbers being larger for ^{3}He and ^{4}He than for ^{20}Ne. There is

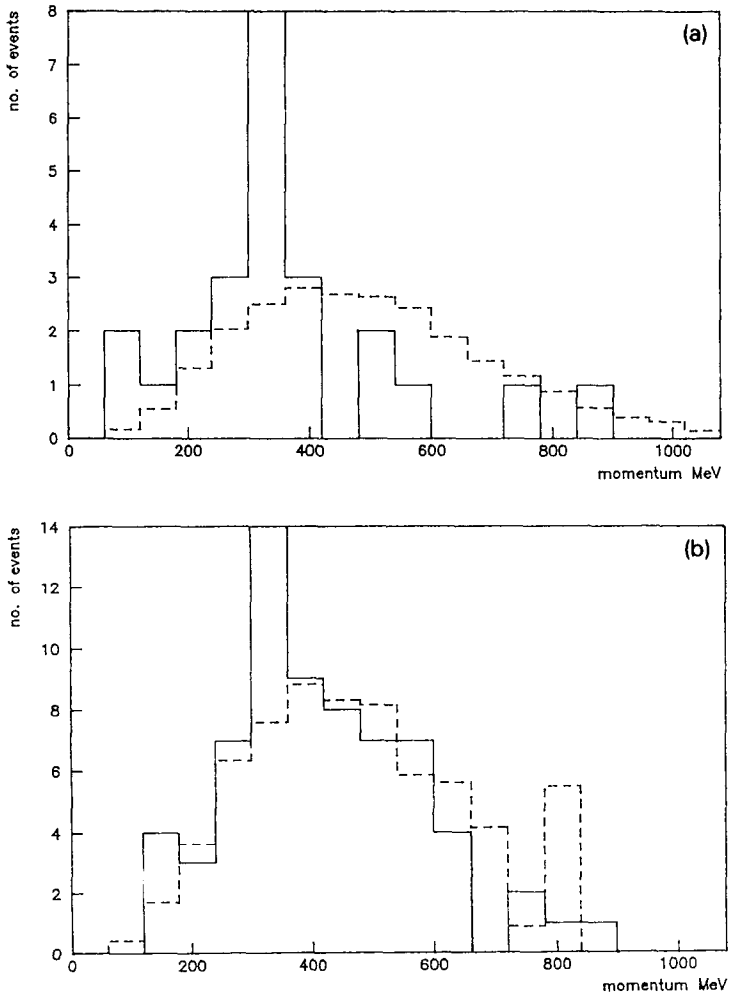

Fig. 24. Experimental momentum spectrum of (a) Λ, (b) K^0_S, in $\bar{p}$ ^{3}He at rest compared to prediction of model I, assumption A. L cut of 1 cm. Solid line: experiment; dashed line: model.

also a momentum dependence of $\langle N_{ch}\rangle(\langle N_-\rangle)$ which is higher (lower) in flight than at rest, at least for $A>4$. A smaller number of negative particles produced means a higher absorption.

The data were compared to simple combinatory calculations based on the extreme assumptions of Λ production only via $B=1$ annihilations or only via $\bar{K}$ rescattering ($B=0$). Both assumptions lead to $R_{K^0_S}(R)$ higher (smaller) than the experimental ones, in agreement with the predictions of the intranuclear cascade model by Cugnon *et al.* [6]). However, $\bar{K}$ rescattering leads to $R_{K^0_S}(R)$ values closer to the experimental ones with a probability of ~40% ($A\geq 4$) that the $\bar{K}$ transforms into a Λ. Moreover, a low $K\bar{K}$ production rate (~3%) is preferred instead of 5-7% from antiproton-

nucleon annihilations [5]). We recall that 3% was found in annihilations on emulsion [21]).

The most relevant feature of the momentum spectra is the difference between the K_S^0 and Λ spectra, and that the Λ and π^- spectra are quite similar. The K_S^0 spectra are shifted towards higher momenta. In $\bar{p}p$ and $\bar{p}d$ all three spectra are similar. We compared the K_S^0 and Λ spectra with the prediction of two extreme phase space (essentially) models, where Λ is produced only via $B=1$ annihilation or only via $\bar{K}$ rescattering ($B=0$).

Two different assumptions were made in each model: no final-state interactions of the produced strange particles (except $\bar{K}$ absorption in one model), or a certain number of final-state interactions introduced. The conclusion is that the Λ spectra are very sensitive (contrary to the K_S^0 spectra) to the model and to the assumptions adopted. The best agreement with the data is obtained with the $B=0$ model with some final rescattering ($\bar{K} \to \Sigma \to \Lambda$).

A review of existing data on neutral strange particles is presented and compared. A clear interpretation of all these data is not yet available, although a number of theoretical papers have dealt with strange-particle production in nuclei.

References

1) J. Rafelski, Phys. Lett. **B207** (1988) 371
2) K. Miyano *et al.*, Phys. Rev. Lett. **53** (1984) 1725
3) J. Cugnon and J. Vandermeulen, Phys. Lett. **B146** (1984) 16;
   J. Cugnon and J. Vandermeulen, Phys. Rev. **C36** (1987)
4) C.M. Ko and R. Yuan, Phys. Lett. **B192** (1987) 31
5) C.B. Dover and P. Koch, Invited talk at the conference on hadronic matter in collision, Tuscon, Arizona, Oct. 1988 and preprint BNL-42105.
6) J. Cugnon *et al.*, Strangeness production in antiproton annihilation on nuclei. Université de Liege, Physique Nucleaire Theorique, Institute de Physique au Sart Tilman, Batiment B.5, B-4000 Liege I (Belgium)
7) D.E. Kharzeev and M.G. Sapozhnikov, preprint E4-88-930, Dubna (1988)
8) J. Cugnon *et al.*, Phys. Rev. **C39** (1989) 181
9) R. Bizzarri *et al.*, Lett. Nuovo Cim. **2** (1969) 431
10) B.Y. Oh *et al.*, Nucl. Phys. **B51** (1973)
11) K. Miyano *et al.*, Phys. Rev. **C38** (1988) 2788
12) F. Balestra *et al.*, Phys. Lett. **B194** (1987) 192
13) Yu. A. Batusov *et al.*, Report 51-89-222, Dubna and Yad. Fiz. **50** (1989) 1524
14) G.T. Condo, T. Handler and H.O. Cohn, Phys. Rev. **C29** (1984) 1531
15) G.A. Smith *et al.*, in The elementary structure of matter, ed. J.-M. Richard *et al.* (Springer, Berlin, 1988) p. 219
16) V.V. Barmin *et al.*, Production of Λ-hyperons and K^0-mesons in annihilation of antiprotons in Xe nuclei at rest and at 0.4–0.9 GeV/c", preprint ITEP (1989) Moscow;
   C. Guaraldo, Antiproton-nucleus interaction at intermediate energies, Nuovo Cim. **A102** (1989)
17) J. Riedlberger *et al.*, Nucl. Phys. **B** [proc. suppl.] **8** (1989) 288
18) F. Balestra *et al.*, Nucl. Instr. Meth. **A234** (1985) 30
19) F. Balestra *et al.*, Nucl. Phys. **A491** (1989) 541
20) F. Balestra *et al.*, Nuovo Cim. **A100** (1988) 323
21) A.G. Ekspong *et al.*, Nucl. Phys. **22** (1961) 353

22) N.J. Digiacomo *et al.*, J. Phys. **G10** (1984) L119
23) J.W. Moulder *et al.*, Nucl. Phys. **B35** (1971) 332
24) J. Roy, in Proc. IVth Int. Symposium on NN interaction, Syracuse, ed. T.E. Kalogeropoulos and K.C. Wali, vol. 1, chap. III, p. 1 (1975)
25) H.-J. Besch *et al.*, Z. Phys. **A292** (1979) 197
26) A.S. Iljinov *et al.*, Nucl. Phys. **A382** (1982) 378
27) E. Bracci *et al.*, CERN-HERA 72-2
28) S.I. Alekhin *et al.*, CERN-HERA 87-01
29) Yu.A. Batusov *et al.*, EuroPhys. Lett. **2** (1986) 115
30) S. Nuguchi *et al.*, Z. Phys. **C24** (1984) 297
31) V. Flaminio *et al.*, CERN-HERA 84-01
32) M.T. Regan *et al.*, Nucl. Phys. **B141** (1978) 65
33) S.J.H. Parkin *et al.*, Nucl. Phys. **B277** (1986) 634
34) R. Bizzarri *et al.* Nuovo Cim. **A22** (1974) 225
35) T.E. Kalogeropoulos, Phys. Rev. **D22** (1980)
36) K. Miyano *et al.*, preprint KEK (1988)
37) R. Armenteros and B. French, High energy physics, ed. E. Burhop (Academic Press, New York, 1969); A. Bettini *et al.*, Nuovo Cim. **A62** (1969) 1038
38) W. Brückner *et al.*, Phys. Lett. **B197** (1987) 463; R.P. Hamilton *et al.*, Phys. Rev. Lett. **44** (1980) 112
39) F. Balestra *et al.*, Nucl. Phys. **A452** (1986) 573